Journal of Computational Physics 325 (2016) 314–337

Contents lists available at ScienceDirect

Journal of Computational Physics

www.elsevier.com/locate/jcp

A fully conservative mimetic discretization of the Navier–Stokes equations in cylindrical coordinates with associated singularity treatment

G.T. Oud [a,*], D.R. van der Heul [a], C. Vuik [a], R.A.W.M. Henkes [b]

[a] Department of Numerical Analysis, Delft University of Technology, Mekelweg 4, 2628 CD, Delft, The Netherlands
[b] Department of Process & Energy, Delft University of Technology, Leeghwaterstraat 21, 2628 CA, Delft, The Netherlands

ARTICLE INFO

Article history:
Received 8 March 2016
Received in revised form 30 July 2016
Accepted 26 August 2016
Available online 31 August 2016

Keywords:
Incompressible flow
Cylindrical coordinates
Mimetic finite difference method
Kinetic energy conservation

ABSTRACT

We present a finite difference discretization of the incompressible Navier–Stokes equations in cylindrical coordinates. This currently is, to the authors' knowledge, the only scheme available that is demonstrably capable of conserving mass, momentum and kinetic energy (in the absence of viscosity) on both uniform and non-uniform grids. Simultaneously, we treat the inherent discretization issues that arise due to the presence of the coordinate singularity at the polar axis. We demonstrate the validity of the conservation claims by performing a number of numerical experiments with the proposed scheme, and we show that it is second order accurate in space using the Method of Manufactured Solutions.

1. Introduction

Although it is generally known that the use of cylindrical coordinates in finite difference methods brings along a number of difficulties, it still appears to be the preferred method of choice for turbulent flow simulations in pipe sections. This is likely due to the relative ease with which higher order approximations can be implemented, and the growing availability of fast flow solvers that benefit from the orthogonality of the structured cylindrical grid. However, an inherent problem in the use of cylindrical coordinates (r, θ, z) is the calculation of variables that lie on or near the polar axis $r = 0$. Looking at the cylindrical Navier–Stokes equations:

$$\frac{1}{r}\frac{\partial (r u_r)}{\partial r} + \frac{1}{r}\frac{\partial u_\theta}{\partial \theta} + \frac{\partial u_z}{\partial z} = 0, \tag{1}$$

and

$$\frac{\partial u_r}{\partial t} + \frac{1}{r}\frac{\partial (r u_r^2)}{\partial r} + \frac{1}{r}\frac{\partial (u_r u_\theta)}{\partial \theta} + \frac{\partial (u_r u_z)}{\partial z} - \frac{u_\theta^2}{r} = -\frac{1}{\rho}\frac{\partial p}{\partial r} + \frac{1}{\rho r}\frac{\partial (r\tau_{rr})}{\partial r} + \frac{1}{\rho r}\frac{\partial \tau_{r\theta}}{\partial \theta} + \frac{1}{\rho}\frac{\partial \tau_{rz}}{\partial z} - \frac{\tau_{\theta\theta}}{\rho r} + g_r, \tag{2}$$

$$\frac{\partial u_\theta}{\partial t} + \frac{1}{r}\frac{\partial (r u_r u_\theta)}{\partial r} + \frac{1}{r}\frac{\partial (u_\theta^2)}{\partial \theta} + \frac{\partial (u_\theta u_z)}{\partial z} + \frac{u_r u_\theta}{r} = -\frac{1}{\rho r}\frac{\partial p}{\partial \theta} + \frac{1}{\rho r}\frac{\partial (r\tau_{r\theta})}{\partial r} + \frac{1}{\rho r}\frac{\partial \tau_{\theta\theta}}{\partial \theta} + \frac{1}{\rho}\frac{\partial \tau_{\theta z}}{\partial z} + \frac{\tau_{r\theta}}{\rho r} + g_\theta, \tag{3}$$

* Principal corresponding author.
E-mail address: g.t.oud@tudelft.nl (G.T. Oud).

http://dx.doi.org/10.1016/j.jcp.2016.08.038
0021-9991/

$$\frac{\partial u_z}{\partial t}+\frac{1}{r}\frac{\partial (r u_r u_z)}{\partial r}+\frac{1}{r}\frac{\partial (u_\theta u_z)}{\partial \theta}+\frac{\partial (u_z^2)}{\partial z}=-\frac{1}{\rho}\frac{\partial p}{\partial z}+\frac{1}{\rho}\frac{\partial (r\tau_{rz})}{r\partial r}+\frac{1}{\rho r}\frac{\partial \tau_{\theta z}}{\partial \theta}+\frac{1}{\rho}\frac{\partial \tau_{zz}}{\partial z}+g_z, \tag{4}$$

with $\mathbf{u}=(u_r,u_\theta,u_z)$ the velocity vector, ρ the flow density, $\mathbf{g}=(g_r,g_\theta,g_z)$ the body force and τ_{ij} the viscous stresses, it would indeed appear that the numerous $1/r$ terms cause the solution to blow up near the polar axis, but, as shown in Morinishi et al. [12], the coordinate singularity is only apparent, and taking rigorous limits shows how the equations actually behave at $r=0$. From a numerical modeling point of view, however, this asymptotic analysis does not provide a clear solution to the singularity problem. Assuming a staggered (Marker-and-Cell) grid [7], the straightforward finite difference discretization of the Navier–Stokes equations in conservative form requires (among others) the radial velocity u_r at $r=0$. In the past, this value was usually estimated in some way using neighboring values. For example, Eggels [4] used an arithmetic mean for the estimate of $u_r(0,\theta_j,z_k)$ using two opposite values:

$$u_r(0,\theta_j,z_k)=\frac{u_r(r_1,\theta_j,z_k)-u_r(r_1,\theta_j+\pi,z_k)}{2}, \tag{5}$$

where the minus sign is necessary because of the orientation (both outwards) of the velocity vectors. This approach, however, yields a multivalued radial velocity. An improved approximation by Fukagata and Kasagi [5] and Griffin et al. [6] leads to a single-valued radial velocity by reconstructing the Cartesian velocity components u_x and u_y at $r=0$ from the neighboring set of velocities and by defining u_r at $r=0$ using the decomposition:

$$u_r(0,\theta,z)=u_x\cos\theta+u_y\sin\theta. \tag{6}$$

A different approach by Verzicco and Orlandi [16] avoids the problem entirely by solving the equations for the quantity ru_r instead of the velocity u_r. For a more extensive overview of existing methods, see Morinishi et al. [12].

Recently, discretizations with improved conservation properties have obtained a growing interest as physically reliable modeling of the finest structures in turbulence requires accurate numerical behavior of the flow energy. In particular, the construction of numerical schemes that conserve kinetic energy for flows with vanishing viscosity has become an active field of research. At a discrete level, conservation of kinetic energy is an attractive property as it assures an unconditionally stable (spatial) discretization. For Cartesian domains, this has lead to a number of schemes that conserve both mass, momentum and kinetic energy on uniform and non-uniform grids, for both low and higher order [11,15]. For cylindrical grids, not much progress seems to have been made on these aspects. Fukagata and Kasagi [5] suggest a highly conserving discretization, but energy is not conserved exactly. Morinishi et al. [12] introduced a new approach where a radial momentum equation is solved *at* $r=0$ after its derivation using l'Hôpital's rule. The authors claim and prove the scheme to be energy conserving in the absence of viscosity for both uniform and non-uniform grids. After a number of tests, however, we noticed disturbances near the radial origin in flows with significant velocity through the origin. Desjardins et al. [3] mention this as well while performing the simulation of an inviscid Lamb-dipole. Furthermore, using a Taylor expansion of the radial momentum equation at the origin, they are able to trace down the problem to an inconsistent discretization, and they ultimately decide to use an averaging method similar to equation (6) for improved accuracy, thereby sacrificing exact energy conservation. None of the mentioned singularity treatments above, except the one of Morinishi et al. [12], appears to conserve energy as they rely on (arithmetic) averaging in obtaining the radial velocity at $r=0$. Hence, the problem of finding an energy conserving scheme for cylindrical coordinates seems to intrinsically contain the necessity for a satisfactory treatment of the singularity at $r=0$.

Most of the methods described above use the notion of a *computational* or *logical* Cartesian space and the *physical* cylindrical space, connected through a Jacobian mapping, to solve the governing equations. The problems involving a radial velocity component at the polar axis arise because this mapping is not bijective at the coordinate $r=0$. Nonetheless, many attempts have been made to derive expressions that include (the inverse of) the Jacobian, an approach the authors believe to likely be ill-fated. Instead, we propose a discretization of the Navier–Stokes equations using a mimetic method that is applied on the cylindrical grid (i.e. in physical space only). Mimetic discretizations [10] are designed to mimic many of the properties of the analytical operators they approximate. They have been shown to be very robust and accurate, but so far they have been surprisingly little used in numerical flow modeling. Abba and Bonaventura [1] derive a mimetic finite difference discretization of the Navier–Stokes equations in Cartesian coordinates, while Barbosa and Daube [2] consider cylindrical coordinates. The latter authors have essentially laid the foundations on which we will proceed. They show how the mimetic operators are derived, albeit for uniform cylindrical grids only. However, their averaging procedure seems to require velocity and vorticity components at locations where they are not defined. It is therefore unlikely that their discretization conserves energy exactly. We will show how to remedy this issue, and then extend the discretization to grids with non-uniform radial and axial node distributions for increased efficiency in turbulence simulations. Using the method of Manufactured Solutions, we show that the resulting discretization is capable of achieving second order accuracy in space and, with a suitable time integration method, is capable of conserving mass, momentum and kinetic energy for both uniform and non-uniform cylindrical grids.

To the authors' knowledge, the proposed method is currently the only approach in the literature that is demonstrated to be fully conservative for cylindrical coordinates. Most related research in this field appears to be focused on increasing spatial accuracy, while we believe that a solid singularity treatment, together with improved conservation properties, should be established first before moving on to increasing global accuracy.

2. Construction of the mimetic operators

Whereas traditional finite difference methods generally focus on minimizing the truncation error, the mimetic finite difference method aims to mimic certain properties of the continuous operators at a discrete level. Nonetheless, results often show that the accuracy and robustness are nearly as good if not better than conventional discretization techniques. The motivation stems from the observation that many mathematical descriptions of physical processes contain the vector derivatives gradient, curl and divergence: consider for example Darcy's law of porous media flow, Maxwell's laws of electromagnetism and the Navier–Stokes equations of fluid flow. The vector derivatives satisfy some well known identities like **curl grad** $= 0$ and **div curl** $= 0$ for scalars and vectors respectively, as well as a number of decomposition and integration by parts theorems. The aim of the mimetic approach is to construct a discrete approximation of the analytical vector calculus by defining discrete vector spaces, inner products and operators, such that the aforementioned identities also hold at the discrete level. In that way, a discrete solution is guaranteed to exhibit many of the underlying properties of the analytical solution.

The approach we follow is based on the work of Hyman and Shashkov [9] and [8], where suitable discrete vector spaces, inner products and derivatives are derived for orthogonal coordinate systems using the finite difference method. Most of the derivations for uniform cylindrical coordinates have already been performed by Barbosa and Daube [2]. We will extend their work by providing the associated expressions for cylindrical grids with non-uniform radial and axial node distributions. An essential result of the rigorous derivation of the mimetic operators is the absence of any problems in the construction of finite difference approximations around the polar axis that are normally encountered when trying to discretize expressions at or near $r = 0$.

We start in section 2.1 by defining the discrete vector spaces, depending on the location of the variables on the MAC grid. Then the metric-independent *natural* vector operations are derived in section 2.2. These provide a limited set of discrete mappings between the discrete vector spaces, but without inverse. The inverse mappings require additional metric data in the form of inner products, which are defined in section 2.3. Finally, the *adjoint* operators are constructed in section 2.4 as the formal adjoints to the natural operators with respect to the associated inner products.

2.1. Definition of the discrete vector spaces

We start by defining a number of discrete vector spaces based on the location of the variables in the computational grid. We assume a non-uniform radial and axial distribution such that $\Delta r = \Delta r_i$ is a function of the radial index i and $\Delta z = \Delta z_k$ is a function of the axial index k. The angular distribution (identified with index j) is assumed to be uniform. A location in the computational grid is represented by a coordinate with multi-index $\mathbf{I} = (i, j, k) \in \mathbb{N}^3$ in combination with the stride vectors $\mathbf{e}_r$, $\mathbf{e}_\theta$ and $\mathbf{e}_z$ defined as:

$$\mathbf{e}_r = \left(\frac{1}{2}, 0, 0\right), \quad \mathbf{e}_\theta = \left(0, \frac{1}{2}, 0\right), \quad \mathbf{e}_z = \left(0, 0, \frac{1}{2}\right). \tag{7}$$

The pressure $p_{\mathbf{I}}$ is located at the cell center $\mathbf{r}_{\mathbf{I}} = (r_i, \theta_j, z_k)$ with coordinates:

$$r_i = \sum_{l=1}^{i} \Delta r_l - \frac{\Delta r_i}{2}, \qquad i \in \{1, \ldots, N_r\}, \tag{8}$$

$$\theta_j = \left(j - \frac{1}{2}\right) \Delta\theta, \qquad j \in \{1, \ldots, N_\theta\}, \tag{9}$$

$$z_k = -\frac{L}{2} + \sum_{l=1}^{k} \Delta z_l - \frac{\Delta z_k}{2}, \qquad k \in \{1, \ldots, N_z\}, \tag{10}$$

where L is the length of the cylinder. For evaluation at the radial cell boundaries, we define $r_{i\pm\frac{1}{2}}$ as $r_{i\pm\frac{1}{2}} = r_i \pm \frac{\Delta r_i}{2}$. The velocity components $u_{r_{I+e_r}}$, $u_{\theta_{I+e_\theta}}$ and $u_{z_{I+e_z}}$ lie orthogonal to the positive cell faces, and the vorticity components $\eta_{I+e_\theta+e_z}$, $\omega_{I+e_r+e_z}$ and $\zeta_{I+e_r+e_\theta}$ lie along the positive cell edges. Fig. 1 shows the location of the scalars and vector components in cylindrical coordinates as they are used in this paper. Note the particular axial vorticity $\zeta_{\frac{1}{2},j,k} = \tilde{\zeta}_k$ located at $r = 0$ and independent of angular index j.

For clarity, we use the same notation as in Hyman and Shashkov [9], with calligraphic letters for spaces with vectors and plain letters for spaces with scalars. The following spaces are used:

- The space $\mathcal{HS}$ of discrete vector functions with components that are defined perpendicular to the cell faces at locations $\mathbf{r}_{\mathbf{I}\pm\mathbf{e}_r}$, $\mathbf{r}_{\mathbf{I}\pm\mathbf{e}_\theta}$ and $\mathbf{r}_{\mathbf{I}\pm\mathbf{e}_z}$ in the domain. The discrete velocity $\mathbf{u} = (u_r, u_\theta, u_z)$ on a staggered grid belongs to this space.
- The space $\mathcal{HL}$ of discrete vector functions with components that are defined on the cell ribs at locations $\mathbf{r}_{\mathbf{I}\pm\mathbf{e}_\theta\pm\mathbf{e}_z}$, $\mathbf{r}_{\mathbf{I}\pm\mathbf{e}_r\pm\mathbf{e}_z}$ and $\mathbf{r}_{\mathbf{I}\pm\mathbf{e}_r\pm\mathbf{e}_\theta}$ in the domain. The discrete vorticity $\boldsymbol{\omega} = (\eta, \omega, \zeta)$ belongs to this space.

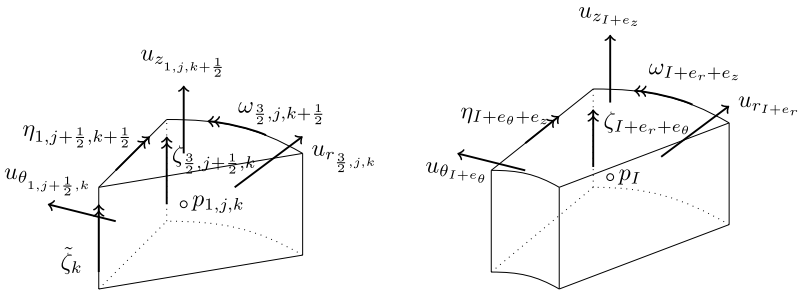

(a) Cells near the axis at (r_1, θ_j, z_k). (b) Cells away from the axis at (r_i, θ_j, z_k).

Fig. 1. Location of the variables in the computational domain.

- The space HC of discrete scalar functions that are defined in the cell centers at locations $\mathbf{r_I}$. The discrete pressure p belongs to this space.
- The space HN of discrete scalar functions that are defined in the cell vertices at locations $\mathbf{r_{I\pm e_r\pm e_\theta\pm e_z}}$, $\mathbf{r_{I\pm e_r\pm e_\theta\pm e_z}}$ and $\mathbf{r_{I\pm e_r\pm e_\theta\pm e_z}}$ in the domain. This space is mentioned for completeness, but it is not used in our approach.

2.2. Definition of the natural vector operations

In Hyman and Shashkov [9], expressions are derived for the discrete divergence **D**, the discrete gradient **G** and the discrete curl **C**. They are defined based on a discrete approximation of their coordinate-independent definitions, i.e.:

$$\nabla \cdot \mathbf{W} := \lim_{V\to 0} \frac{\oint_{\partial V} (\mathbf{W}, \mathbf{n})\, \mathrm{d}S}{V}, \tag{11}$$

$$(\nabla u, \mathbf{n}) := \frac{\partial u}{\partial n}, \tag{12}$$

$$(\mathbf{n}, \nabla \times \mathbf{W}) := \lim_{S\to 0} \frac{\oint_l (\mathbf{W}, \mathbf{l})\, \mathrm{d}l}{S}, \tag{13}$$

for some volume V with boundary ∂V, normal vector $\mathbf{n}$ and surface S with boundary l. The divergence operator **D** is the natural[1] mapping $\mathbf{D} : \mathcal{HS} \to HC$. The gradient operator **G** is the natural mapping $\mathbf{G} : HN \to \mathcal{HL}$, while the curl operator **C** is the natural mapping $\mathbf{C} : \mathcal{HL} \to \mathcal{HS}$. Combined, the natural operators **G**, **C** and **D** form the sequence:

$$HN \xrightarrow{\mathbf{G}} \mathcal{HL} \xrightarrow{\mathbf{C}} \mathcal{HS} \xrightarrow{\mathbf{D}} HC. \tag{14}$$

The construction of the natural operators **D** and **C** is shown below (for our purposes, we do not need **G**). The resulting operators satisfy (among others) the well known vector identities (for proofs of this, see Hyman and Shashkov [9]):

$$\mathbf{DC} : \mathcal{HL} \to HC, \quad \mathbf{DC} \equiv 0, \qquad \mathbf{CG} : HN \to \mathcal{HS}, \quad \mathbf{CG} \equiv 0. \tag{15}$$

Notice that the resulting expressions, although derived from mimetic principles, are in fact often equal to the classical finite difference discretizations of the gradient, curl and divergence operators in cylindrical coordinates at the computational cell centers. This shows that a mimetic approach does not necessarily lead to different discretization results, but it does provide additional insight and motivation.

The divergence operator $\mathbf{D} : \mathcal{HS} \to HC$ The natural divergence operator $\mathbf{D} : \mathcal{HS} \to HC$ follows from the coordinate-independent formulation of Gauss' divergence theorem:

$$\nabla \cdot \mathbf{W} := \lim_{V\to 0} \frac{1}{V} \oint\!\!\oint_{\partial V} (\mathbf{W}, \mathbf{n})\, \mathrm{d}S, \tag{16}$$

where $\mathbf{n}$ is the unit outward normal to the boundary ∂V and $\mathbf{W} : \mathbb{R}^n \to \mathbb{R}^n$ is a differentiable vector field. For a cylindrical cell away from the axis $r = 0$, the discrete approximation **Du** to equation (16) becomes:

[1] The mappings are considered natural because the location of the variables on the staggered grid allows straightforward discrete evaluations of their analytical definitions, i.e. Gauss' theorem (for the divergence) and Stokes' theorem (for the curl).

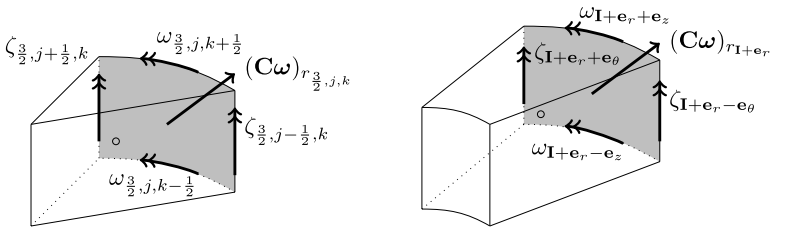

(a) Radial component at the axis. (b) Radial component away from the axis.

Fig. 2. Surface for the determination of the radial component of the curl operator $\mathbf{C}:\mathcal{HL}\to\mathcal{HS}$.

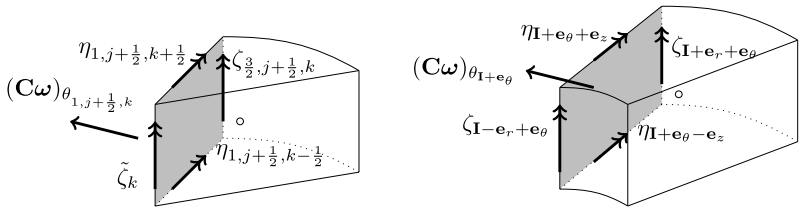

(a) Angular component at the axis. (b) Angular component away from the axis.

Fig. 3. Surface for the determination of the angular component of the curl operator $\mathbf{C}:\mathcal{HL}\to\mathcal{HS}$.

$$(\mathbf{Du})_{\mathbf{I}} = \frac{1}{r_i\Delta r_i\Delta\theta\Delta z_k}\Big[\Delta\theta\Delta z_k(r_{i+\frac{1}{2}}u_{r_{\mathbf{I}+\mathbf{e}_r}} - r_{i-\frac{1}{2}}u_{r_{\mathbf{I}-\mathbf{e}_r}}) + \Delta r_i\Delta z_k(u_{\theta_{\mathbf{I}+\mathbf{e}_\theta}} - u_{\theta_{\mathbf{I}-\mathbf{e}_\theta}}) + r_i\Delta r_i\Delta\theta(u_{z_{\mathbf{I}+\mathbf{e}_z}} - u_{z_{\mathbf{I}-\mathbf{e}_z}})\Big] \tag{17}$$

$$= \frac{r_{i+\frac{1}{2}}u_{r_{\mathbf{I}+\mathbf{e}_r}} - r_{i-\frac{1}{2}}u_{r_{\mathbf{I}-\mathbf{e}_r}}}{r_i\Delta r_i} + \frac{u_{\theta_{\mathbf{I}+\mathbf{e}_\theta}} - u_{\theta_{\mathbf{I}-\mathbf{e}_\theta}}}{r_i\Delta\theta} + \frac{u_{z_{\mathbf{I}+\mathbf{e}_z}} - u_{z_{\mathbf{I}-\mathbf{e}_z}}}{\Delta z_k}, \tag{18}$$

for some discrete vector $\mathbf{u} = (u_r, u_\theta, u_z) \in \mathcal{HS}$. Notice that this result corresponds with the classical finite difference approximation of the cylindrical divergence:

$$\frac{1}{r}\frac{\partial(ru_r)}{\partial r} + \frac{1}{r}\frac{\partial u_\theta}{\partial\theta} + \frac{\partial u_z}{\partial z}. \tag{19}$$

For cells at the polar axis with $i = 1$ where $r_{\frac{1}{2}} = 0$, the discrete operator reduces without issues to:

$$(\mathbf{Du})_{\mathbf{I},i=1} = \frac{2u_{r_{\mathbf{I}+\mathbf{e}_r}}}{\Delta r_i} + \frac{2\left(u_{\theta_{\mathbf{I}+\mathbf{e}_\theta}} - u_{\theta_{\mathbf{I}-\mathbf{e}_\theta}}\right)}{\Delta r_i\Delta\theta} + \frac{u_{z_{\mathbf{I}+\mathbf{e}_z}} - u_{z_{\mathbf{I}-\mathbf{e}_z}}}{\Delta z_k}, \tag{20}$$

where on the right-hand side the i-component in the multi-index $\mathbf{I}$ is equal to 1.

The curl operator $\mathbf{C}:\mathcal{HL}\to\mathcal{HS}$ The natural curl operator $\mathbf{C}:\mathcal{HL}\to\mathcal{HS}$ follows from the coordinate-independent formulation of Stokes' circulation theorem:

$$(\mathbf{n}, \nabla\times\mathbf{W}) := \lim_{S\to 0}\frac{1}{S}\oint_l(\mathbf{W},\mathbf{l})\,\mathrm{d}l, \tag{21}$$

where S is the surface enclosed by the closed curve l, $\mathbf{n}$ is the unit outward normal to S, $\mathbf{l}$ is the unit tangential vector to l and $\mathbf{W}:\mathbb{R}^n\to\mathbb{R}^n$ is a differentiable vector field. Let $\boldsymbol{\omega} = (\eta,\omega,\zeta)$ be a discrete vector in $\mathcal{HL}$ with its components located as shown in Fig. 1. Then for the radial component $(\mathbf{C}\boldsymbol{\omega})_r$, the curve l around the surface S is defined as the boundary of the gray plane in Fig. 2 for both types of cells.

The radial component of $\mathbf{C}\boldsymbol{\omega}$ is then approximated as:

$$(\mathbf{C}\boldsymbol{\omega})_{r_{\mathbf{I}+\mathbf{e}_r}} = \frac{1}{r_{i+\frac{1}{2}}\Delta\theta\Delta z_k}\Big[r_{i+\frac{1}{2}}\Delta\theta(-\omega_{\mathbf{I}+\mathbf{e}_r+\mathbf{e}_z} + \omega_{\mathbf{I}+\mathbf{e}_r-\mathbf{e}_z}) + \Delta z_k(\zeta_{\mathbf{I}+\mathbf{e}_r+\mathbf{e}_\theta} - \zeta_{\mathbf{I}+\mathbf{e}_r-\mathbf{e}_\theta})\Big] \tag{22}$$

$$= \frac{\zeta_{\mathbf{I}+\mathbf{e}_r+\mathbf{e}_\theta} - \zeta_{\mathbf{I}+\mathbf{e}_r-\mathbf{e}_\theta}}{r_{i+\frac{1}{2}}\Delta\theta} - \frac{\omega_{\mathbf{I}+\mathbf{e}_r+\mathbf{e}_z} - \omega_{\mathbf{I}+\mathbf{e}_r-\mathbf{e}_z}}{\Delta z_k}. \tag{23}$$

For the angular component $(\mathbf{C}\boldsymbol{\omega})_\theta$, the curve l around the surface S is defined as the boundary of the gray plane in Fig. 3.

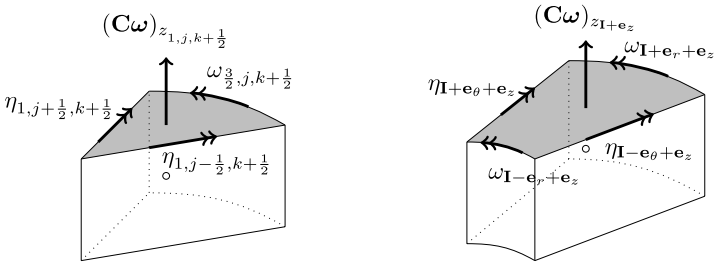

(a) Axial component at the axis. (b) Axial component away from the axis.

Fig. 4. Surface for the determination of the axial component of the curl operator $\mathbf{C}: \mathcal{HL} \to \mathcal{HS}$.

The angular component is then approximated as:

$$(\mathbf{C}\boldsymbol{\omega})_{\theta_{\mathbf{I}+\mathbf{e}_\theta}} = \frac{1}{\Delta r_i \Delta z_k}\Big[\Delta r_i(\eta_{\mathbf{I}+\mathbf{e}_\theta+\mathbf{e}_z} - \eta_{\mathbf{I}+\mathbf{e}_\theta-\mathbf{e}_z}) + \Delta z_k(-\zeta_{\mathbf{I}+\mathbf{e}_r+\mathbf{e}_\theta} + \zeta_{\mathbf{I}-\mathbf{e}_r+\mathbf{e}_\theta})\Big] \tag{24}$$

$$= \frac{\eta_{\mathbf{I}+\mathbf{e}_\theta+\mathbf{e}_z} - \eta_{\mathbf{I}+\mathbf{e}_\theta-\mathbf{e}_z}}{\Delta z_k} - \frac{\zeta_{\mathbf{I}+\mathbf{e}_r+\mathbf{e}_\theta} - \zeta_{\mathbf{I}-\mathbf{e}_r+\mathbf{e}_\theta}}{\Delta r_i}. \tag{25}$$

Finally, for the axial component $(\mathbf{C}\boldsymbol{\omega})_z$, the curve l around the surface S is defined as the boundary of the gray plane shown in Fig. 4. The axial component is approximated as:

$$(\mathbf{C}\boldsymbol{\omega})_{z_{\mathbf{I}+\mathbf{e}_z}} = \frac{1}{r_i \Delta r_i \Delta\theta}\Big[\Delta r_i(-\eta_{\mathbf{I}+\mathbf{e}_\theta+\mathbf{e}_z} + \eta_{\mathbf{I}-\mathbf{e}_\theta+\mathbf{e}_z}) + \Delta\theta(r_{i+\frac{1}{2}}\omega_{\mathbf{I}+\mathbf{e}_r+\mathbf{e}_z} - r_{i-\frac{1}{2}}\omega_{\mathbf{I}-\mathbf{e}_r+\mathbf{e}_z})\Big] \tag{26}$$

$$= \frac{1}{r_i}\left[\frac{r_{i+\frac{1}{2}}\omega_{\mathbf{I}+\mathbf{e}_r+\mathbf{e}_z} - r_{i-\frac{1}{2}}\omega_{\mathbf{I}-\mathbf{e}_r+\mathbf{e}_z}}{\Delta r_i} - \frac{\eta_{\mathbf{I}+\mathbf{e}_\theta+\mathbf{e}_z} - \eta_{\mathbf{I}-\mathbf{e}_\theta+\mathbf{e}_z}}{\Delta\theta}\right]. \tag{27}$$

Notice that the non-existence of the angular vorticity element ω for axis cells where $i = 1$ is naturally resolved by the multiplication with $r_{\frac{1}{2}} = 0$. Hence, for axis cells, the expression reduces to:

$$(\mathbf{C}\boldsymbol{\omega})_{z_{\mathbf{1},i=1}} = \frac{2\omega_{\mathbf{I}+\mathbf{e}_r+\mathbf{e}_z}}{\Delta r_i} - \frac{2\left(\eta_{\mathbf{I}+\mathbf{e}_\theta+\mathbf{e}_z} - \eta_{\mathbf{I}-\mathbf{e}_\theta-\mathbf{e}_z}\right)}{\Delta r_i \Delta\theta}, \tag{28}$$

where on the right-hand side the i-component of the multi-index $\mathbf{I}$ is equal to 1.

2.3. Definition of the discrete inner products

To derive the adjoint operators, we need the notion of inner products on the discrete vector spaces. These are defined as approximations of the continuous L^2-inner product, using either the (second order accurate) Midpoint or Trapezoidal integration rule.

An inner product on HC For the space HC, the inner product $(\cdot,\cdot)_{HC}: HC \times HC \to \mathbb{R}$ is defined as:

$$(u, v)_{HC} := \sum_{\mathbf{I}} u_{\mathbf{I}} v_{\mathbf{I}} r_i \Delta r_i \Delta\theta \Delta z_k, \tag{29}$$

where u and v are two discrete scalar functions defined in the cell centers.

An inner product on $\mathcal{HS}$ For the space $\mathcal{HS}$, the inner product $(\cdot,\cdot)_{\mathcal{HS}}: \mathcal{HS} \times \mathcal{HS} \to \mathbb{R}$ is defined as:

$$(\mathbf{u}, \mathbf{v})_{\mathcal{HS}} := \sum_{\mathbf{I}} \frac{\Delta r_i \Delta\theta \Delta z_k}{2}\Big[r_{i-\frac{1}{2}} u_{\mathbf{I}-\mathbf{e}_r} v_{\mathbf{I}-\mathbf{e}_r} + r_{i+\frac{1}{2}} u_{\mathbf{I}+\mathbf{e}_r} v_{\mathbf{I}+\mathbf{e}_r} + r_i(u_{\mathbf{I}-\mathbf{e}_\theta} v_{\mathbf{I}-\mathbf{e}_\theta} + u_{\mathbf{I}+\mathbf{e}_\theta} v_{\mathbf{I}+\mathbf{e}_\theta})$$
$$+ r_i(u_{\mathbf{I}-\mathbf{e}_z} v_{\mathbf{I}-\mathbf{e}_z} + u_{\mathbf{I}+\mathbf{e}_z} v_{\mathbf{I}+\mathbf{e}_z})\Big]. \tag{30}$$

An inner product on $\mathcal{HL}$ The inner product $(\cdot,\cdot)_{\mathcal{HL}}: \mathcal{HL} \times \mathcal{HL} \to \mathbb{R}$ of two vectors $\boldsymbol{\omega} = (\eta, \omega, \zeta)$ and $\bar{\boldsymbol{\omega}} = (\bar{\eta}, \bar{\omega}, \bar{\zeta})$ in $\mathcal{HL}$ is given by

$$
\begin{aligned}
(\boldsymbol{\omega},\bar{\boldsymbol{\omega}})_{\mathcal{HL}} := \sum_{\mathbf{I},i\neq 1} \frac{\Delta r_i \Delta\theta \Delta z_k}{2} \cdot \Bigg[& r_i \frac{\eta_{\mathbf{I}-\mathbf{e}_\theta-\mathbf{e}_z}\bar{\eta}_{\mathbf{I}-\mathbf{e}_\theta-\mathbf{e}_z} + \eta_{\mathbf{I}+\mathbf{e}_\theta-\mathbf{e}_z}\bar{\eta}_{\mathbf{I}+\mathbf{e}_\theta-\mathbf{e}_z}}{2} \\
& + r_i \frac{\eta_{\mathbf{I}-\mathbf{e}_\theta+\mathbf{e}_z}\bar{\eta}_{\mathbf{I}-\mathbf{e}_\theta+\mathbf{e}_z} + \eta_{\mathbf{I}+\mathbf{e}_\theta+\mathbf{e}_z}\bar{\eta}_{\mathbf{I}+\mathbf{e}_\theta+\mathbf{e}_z}}{2} \\
& + r_{i-\frac{1}{2}} \frac{\omega_{\mathbf{I}-\mathbf{e}_r-\mathbf{e}_z}\bar{\omega}_{\mathbf{I}-\mathbf{e}_r-\mathbf{e}_z} + \omega_{\mathbf{I}-\mathbf{e}_r+\mathbf{e}_z}\bar{\omega}_{\mathbf{I}-\mathbf{e}_r+\mathbf{e}_z}}{2} \\
& + r_{i+\frac{1}{2}} \frac{\omega_{\mathbf{I}+\mathbf{e}_r-\mathbf{e}_z}\bar{\omega}_{\mathbf{I}+\mathbf{e}_r-\mathbf{e}_z} + \omega_{\mathbf{I}+\mathbf{e}_r+\mathbf{e}_z}\bar{\omega}_{\mathbf{I}+\mathbf{e}_r+\mathbf{e}_z}}{2} \\
& + \left(\frac{r_{i-1}+r_i}{2}\right)\left(\frac{\zeta_{\mathbf{I}-\mathbf{e}_r-\mathbf{e}_\theta}\bar{\zeta}_{\mathbf{I}-\mathbf{e}_r-\mathbf{e}_\theta} + \zeta_{\mathbf{I}-\mathbf{e}_r+\mathbf{e}_\theta}\bar{\zeta}_{\mathbf{I}-\mathbf{e}_r+\mathbf{e}_\theta}}{2}\right) \\
& + \left(\frac{r_i+r_{i+1}}{2}\right)\left(\frac{\zeta_{\mathbf{I}+\mathbf{e}_r-\mathbf{e}_\theta}\bar{\zeta}_{\mathbf{I}+\mathbf{e}_r-\mathbf{e}_\theta} + \zeta_{\mathbf{I}+\mathbf{e}_r+\mathbf{e}_\theta}\bar{\zeta}_{\mathbf{I}+\mathbf{e}_r+\mathbf{e}_\theta}}{2}\right) \Bigg] \\
& + \sum_{\mathbf{I},i=1} \frac{\Delta r_i \Delta\theta \Delta z_k}{2} \cdot \Bigg[r_i \frac{\eta_{\mathbf{I}-\mathbf{e}_\theta-\mathbf{e}_z}\bar{\eta}_{\mathbf{I}-\mathbf{e}_\theta-\mathbf{e}_z} + \eta_{\mathbf{I}+\mathbf{e}_\theta-\mathbf{e}_z}\bar{\eta}_{\mathbf{I}+\mathbf{e}_\theta-\mathbf{e}_z}}{2} \\
& + r_i \frac{\eta_{\mathbf{I}-\mathbf{e}_\theta+\mathbf{e}_z}\bar{\eta}_{\mathbf{I}-\mathbf{e}_\theta+\mathbf{e}_z} + \eta_{\mathbf{I}+\mathbf{e}_\theta+\mathbf{e}_z}\bar{\eta}_{\mathbf{I}+\mathbf{e}_\theta+\mathbf{e}_z}}{2} \\
& + r_{i+\frac{1}{2}} \frac{\omega_{\mathbf{I}+\mathbf{e}_r-\mathbf{e}_z}\bar{\omega}_{\mathbf{I}+\mathbf{e}_r-\mathbf{e}_z} + \omega_{\mathbf{I}+\mathbf{e}_r+\mathbf{e}_z}\bar{\omega}_{\mathbf{I}+\mathbf{e}_r+\mathbf{e}_z}}{2} \\
& + \frac{r_i}{2}\tilde{\zeta}_k\tilde{\bar{\zeta}}_k + \left(\frac{r_i+r_{i+1}}{2}\right)\left(\frac{\zeta_{\mathbf{I}+\mathbf{e}_r-\mathbf{e}_\theta}\bar{\zeta}_{\mathbf{I}+\mathbf{e}_r-\mathbf{e}_\theta} + \zeta_{\mathbf{I}+\mathbf{e}_r+\mathbf{e}_\theta}\bar{\zeta}_{\mathbf{I}+\mathbf{e}_r+\mathbf{e}_\theta}}{2}\right) \Bigg].
\end{aligned}
\tag{31}
$$

Notice that for $i = 1$, the degeneracy of the cell has been taken into account: for the angular components ω and $\bar{\omega}$, this follows naturally by multiplication with $r_{\frac{1}{2}} = 0$. For the axial components ζ and $\bar{\zeta}$, the expression is altered to accommodate the collapse of the cell face at $r = 0$. It can be verified that all three discrete inner products satisfy the required symmetry, linearity and positive-definiteness properties.

2.4. Definition of the adjoint vector operations

The discrete operators derived in section 2.2 only allow the trivial successive applications **CG** and **DC**, which are identically zero. Second order operators like **DG** of a scalar and **CC** of a vector are not possible because the range does not equal the domain of the consecutive first order operators. To overcome this, the adjoint operators $\overline{\mathbf{D}}$, $\overline{\mathbf{G}}$ and $\overline{\mathbf{C}}$ are derived using the Support Operator Method [14]. By choosing a *prime* (natural) operator, the associated *derived* (adjoint) operator follows from the discrete inner product in combination with the identities:

$$\mathbf{D} = -\mathbf{G}^*, \qquad \mathbf{C} = \mathbf{C}^*, \tag{32}$$

where the $*$ denotes the adjoint with respect to the associated inner product. More specifically, starting with the natural operator $\mathbf{D} : \mathcal{HS} \to HC$, the operator $\overline{\mathbf{G}} : HC \to \mathcal{HS}$ is defined through:

$$(\mathbf{Du}, v)_{HC} = -\left(\mathbf{u}, \overline{\mathbf{G}}v\right)_{\mathcal{HS}}, \tag{33}$$

for any $\mathbf{u} \in \mathcal{HS}$ and $v \in HC$. In a similar way, expressions can be derived for the derived divergence operator $\overline{\mathbf{D}} : \mathcal{HL} \to HN$ and a derived curl operator $\overline{\mathbf{C}} : \mathcal{HS} \to \mathcal{HL}$ through:

$$(\mathbf{G}u, \mathbf{v})_{\mathcal{HL}} = -\left(u, \overline{\mathbf{D}}\mathbf{v}\right)_{HN}, \qquad u \in HN, \mathbf{v} \in \mathcal{HL}, \tag{34}$$

$$(\mathbf{Cu}, \mathbf{v})_{\mathcal{HS}} = \left(\mathbf{u}, \overline{\mathbf{C}}\mathbf{v}\right)_{\mathcal{HL}}, \qquad \mathbf{u} \in \mathcal{HL}, \mathbf{v} \in \mathcal{HS}. \tag{35}$$

With both natural and adjoint discrete operators, it is now possible to discretize combinations like:

$$\mathbf{D}\overline{\mathbf{G}} : HC \to HC, \qquad \overline{\mathbf{D}}\mathbf{G} : HN \to HN, \tag{36}$$

$$\mathbf{C}\overline{\mathbf{C}} : \mathcal{HS} \to \mathcal{HS}, \qquad \overline{\mathbf{C}}\mathbf{C} : \mathcal{HL} \to \mathcal{HL}, \tag{37}$$

$$\mathbf{G}\overline{\mathbf{D}} : \mathcal{HL} \to \mathcal{HL}, \qquad \overline{\mathbf{G}}\mathbf{D} : \mathcal{HS} \to \mathcal{HS}, \tag{38}$$

and even the vector Laplacian. It is shown in Hyman and Shashkov [8] that the discrete operators satisfy several additional important theorems from vector calculus. Just like the natural operators, the adjoint operators $\overline{\mathbf{G}}$, $\overline{\mathbf{C}}$ and $\overline{\mathbf{D}}$ form a sequence (but in reversed direction):

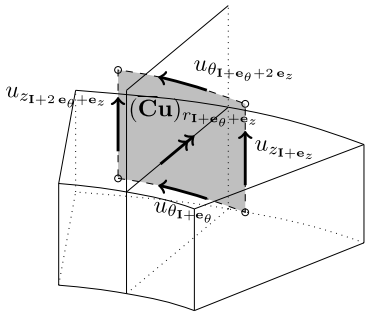

Fig. 5. Surface for the determination of the radial component of the curl operator $\overline{\mathbf{C}}: \mathcal{HS} \to \mathcal{HL}$.

$$HC \xrightarrow{\overline{\mathbf{G}}} \mathcal{HS} \xrightarrow{\overline{\mathbf{C}}} \mathcal{HL} \xrightarrow{\overline{\mathbf{D}}} HN. \tag{39}$$

We will now construct the adjoint operators $\overline{\mathbf{G}}$ and $\overline{\mathbf{C}}$ for cylindrical grids with a non-uniform radial and axial distribution (we do not require $\overline{\mathbf{D}}$). In addition, we will prove that the constructed adjoint operators are indeed the formal adjoints of the associated natural operators with respect to their inner products.

The gradient operator $\overline{\mathbf{G}}: HC \to \mathcal{HS}$ The components of the gradient operator $\overline{\mathbf{G}}: HC \to \mathcal{HS}$ are defined as:

$$\left(\overline{\mathbf{G}}p\right)_{r_{\mathbf{I}+\mathbf{e}_r}} = \frac{2(p_{\mathbf{I}+2\mathbf{e}_r} - p_{\mathbf{I}})}{\Delta r_i + \Delta r_{i+1}} \tag{40}$$

$$\left(\overline{\mathbf{G}}p\right)_{\theta_{\mathbf{I}+\mathbf{e}_\theta}} = \frac{p_{\mathbf{I}+2\mathbf{e}_\theta} - p_{\mathbf{I}}}{r_i \Delta\theta} \tag{41}$$

$$\left(\overline{\mathbf{G}}p\right)_{z_{\mathbf{I}+\mathbf{e}_z}} = \frac{2(p_{\mathbf{I}+2\mathbf{e}_z} - p_{\mathbf{I}})}{\Delta z_k + \Delta z_{k+1}}, \tag{42}$$

for some scalar $p \in HC$.

Proposition 2.1. *For any $p \in HC$ and $\mathbf{u} \in \mathcal{HS}$ on an infinite domain, it holds that $(\mathbf{Du}, p)_{HC} = -(\mathbf{u}, \overline{\mathbf{G}}p)_{\mathcal{HS}}$.*

Proof. See Appendix A. □

On finite domains, the boundary conditions on HC and $\mathcal{HS}$ need to be chosen consistently in order for expression (33) to hold exactly. We assume a finite cylindrical domain of radius R and length L with an associated grid that includes a single layer of ghost cells at both the radial and axial walls. The inner product $(\mathbf{Du}, p)_{HC}$ contains only internal values of p, while the discrete gradient in $(\mathbf{u}, \overline{\mathbf{G}}p)_{\mathcal{HS}}$ also includes values of p in the layer of ghost cells. Consider now a computational cell that shares a face with the cylinder boundary. The contribution of the adjacent ghost cell to $(\mathbf{u}, \overline{\mathbf{G}}p)_{\mathcal{HS}}$ can be removed by actively setting the discrete gradient of p at the boundary to zero. But for consistency in the product $(\mathbf{Du}, p)_{HC}$, the value of the component of $\mathbf{u}$ normal to the boundary then has to be set to zero (compare the contributions in equations (108) and (109)). This combination of Neumann and Dirichlet boundary conditions for p and $\mathbf{u}$ respectively are the well known expressions for the simulation of a solid wall without penetration when p and $\mathbf{u}$ represent the pressure and the flow velocity respectively.

A second case involves periodic wall conditions. For simplicity, we assume that the axial boundaries at $z = \pm L/2$ are periodic, so that the layers of ghost cells at these walls coincide with the first and last slices of the internal cells of the grid. With minor adjustments, the same strategy as the proof for an infinite domain can be used to demonstrate that in this case the inner products are also equal. Hence, on finite domains, Proposition 2.1 is in particular valid for the common situation of cylindrical pipe flows with solid or periodic walls.

The curl operator $\overline{\mathbf{C}}: \mathcal{HS} \to \mathcal{HL}$ The adjoint curl operator $\overline{\mathbf{C}}$ is derived according to equation (21) in a similar way as the natural curl operator $\mathbf{C}$. It will be shown that the resulting expressions for the components of $\overline{\mathbf{C}}$ are indeed the adjoints of the associated components of $\mathbf{C}$ with respect to the discrete inner product $(\cdot,\cdot)_{\mathcal{HL}}$. Throughout the derivation, let $\mathbf{u} = (u_r, u_\theta, u_z)$ be a discrete vector in $\mathcal{HS}$. Then for the radial component of the adjoint curl operator $(\overline{\mathbf{C}}\mathbf{u})_r$, the surface S is defined as the gray plane in Fig. 5. The component of the discrete curl operator $\overline{\mathbf{C}}$ in the radial direction then follows as:

$$(\overline{\mathbf{C}}\mathbf{u})_{r_{\mathbf{I}+\mathbf{e}_\theta+\mathbf{e}_z}} = \frac{2}{r_i \Delta\theta(\Delta z_k + \Delta z_{k+1})}\left[\frac{\Delta z_k + \Delta z_{k+1}}{2}(u_{z_{\mathbf{I}+2\mathbf{e}_\theta+\mathbf{e}_z}} - u_{z_{\mathbf{I}+\mathbf{e}_z}}) + r_i \Delta\theta(-u_{\theta_{\mathbf{I}+\mathbf{e}_\theta+2\mathbf{e}_z}} + u_{\theta_{\mathbf{I}+\mathbf{e}_\theta}})\right] \tag{43}$$

$$= \frac{u_{z_{\mathbf{I}+2\mathbf{e}_\theta+\mathbf{e}_z}} - u_{z_{\mathbf{I}+\mathbf{e}_z}}}{r_i \Delta\theta} - \frac{2(u_{\theta_{\mathbf{I}+\mathbf{e}_\theta+2\mathbf{e}_z}} - u_{\theta_{\mathbf{I}+\mathbf{e}_\theta}})}{\Delta z_k + \Delta z_{k+1}}. \tag{44}$$

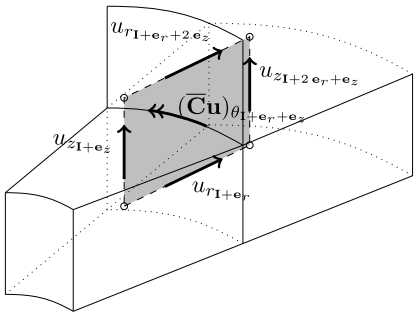

Fig. 6. Surface for the determination of the angular component of the curl operator $\overline{\mathbf{C}}: \mathcal{HS} \to \mathcal{HL}$.

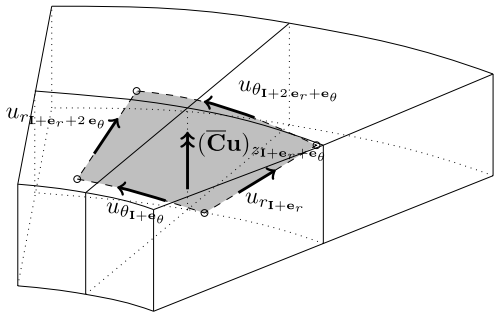

Fig. 7. Surface for the determination of the axial component of the curl operator $\overline{\mathbf{C}}: \mathcal{HS} \to \mathcal{HL}$.

For the angular component, the surface is defined as in Fig. 6. The component of the discrete curl operator $(\overline{\mathbf{C}}\mathbf{u})_\theta$ in the angular direction is defined as:

$$(\overline{\mathbf{C}}\mathbf{u})_{\theta_{\mathbf{I}+\mathbf{e}_r+\mathbf{e}_z}} = \frac{4}{(\Delta r_i + \Delta r_{i+1})(\Delta z_k + \Delta z_{k+1})}\left[\frac{\Delta z_k + \Delta z_{k+1}}{2}\cdot\right. \tag{45}$$

$$\left.\left(u_{z_{\mathbf{I}+\mathbf{e}_z}} - u_{z_{\mathbf{I}+2\mathbf{e}_r+\mathbf{e}_z}}\right) + \frac{\Delta r_i + \Delta r_{i+1}}{2}\left(u_{r_{\mathbf{I}+\mathbf{e}_r+2\mathbf{e}_z}} - u_{r_{\mathbf{I}+\mathbf{e}_r}}\right)\right]$$

$$= \frac{2(u_{r_{\mathbf{I}+\mathbf{e}_r+2\mathbf{e}_z}} - u_{r_{\mathbf{I}+\mathbf{e}_r}})}{\Delta z_k + \Delta z_{k+1}} - \frac{2(u_{z_{\mathbf{I}+2\mathbf{e}_r+\mathbf{e}_z}} - u_{z_{\mathbf{I}+\mathbf{e}_z}})}{\Delta r_i + \Delta r_{i+1}}. \tag{46}$$

For the axial component for cells away from the axis, the surface is defined as in Fig. 7. In this case, the component of the discrete curl operator $(\overline{\mathbf{C}}\mathbf{u})_z$ in the axial direction is defined as:

$$(\overline{\mathbf{C}}\mathbf{u})_{z_{\mathbf{I}+\mathbf{e}_r+\mathbf{e}_\theta}} = \frac{4}{(r_i + r_{i+1})(\Delta r_i + \Delta r_{i+1})\Delta\theta}\left[\frac{\Delta r_i + \Delta r_{i+1}}{2}\cdot\right. \tag{47}$$

$$\left.\left(u_{r_{\mathbf{I}+\mathbf{e}_r}} - u_{r_{\mathbf{I}+\mathbf{e}_r+2\mathbf{e}_\theta}}\right) + \Delta\theta\left(r_{i+1}u_{\theta_{\mathbf{I}+2\mathbf{e}_r+\mathbf{e}_\theta}} - r_i u_{\theta_{\mathbf{I}+\mathbf{e}_\theta}}\right)\right]$$

$$= \frac{2}{r_i + r_{i+1}}\left[\frac{2\left(r_{i+1}u_{\theta_{\mathbf{I}+2\mathbf{e}_r+\mathbf{e}_\theta}} - r_i u_{\theta_{\mathbf{I}+\mathbf{e}_\theta}}\right)}{\Delta r_i + \Delta r_{i+1}} - \frac{u_{r_{\mathbf{I}+\mathbf{e}_r+2\mathbf{e}_\theta}} - u_{r_{\mathbf{I}+\mathbf{e}_r}}}{\Delta\theta}\right]. \tag{48}$$

For the cells near the axis, the surface S is defined as in Fig. 8. For these cells, the component of the discrete curl operator $\overline{\mathbf{C}}$ in the axial direction:

$$(\overline{\mathbf{C}}\mathbf{u})_{z_k} = \frac{8}{N_\theta \Delta r_1^2 \Delta\theta}\sum_{j=1}^{N_\theta}\frac{\Delta r_1}{2}\Delta\theta u_{\theta_{1,j+\frac{1}{2},k}} = \frac{4}{\Delta r_1}\frac{1}{N_\theta}\sum_{j=1}^{N_\theta}u_{\theta_{1,j+\frac{1}{2},k}}. \tag{49}$$

Proposition 2.2. *For any $\boldsymbol{\omega} \in \mathcal{HL}$ and $\mathbf{u} \in \mathcal{HS}$ on an infinite domain, it holds that $(\mathbf{C}\boldsymbol{\omega}, \mathbf{u})_{\mathcal{HS}} = (\boldsymbol{\omega}, \overline{\mathbf{C}}\mathbf{u})_{\mathcal{HL}}$.*

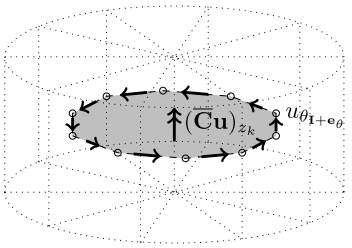

Fig. 8. Surface for the determination of the axial component of the curl operator $\overline{\mathbf{C}}: \mathcal{HS} \to \mathcal{HL}$.

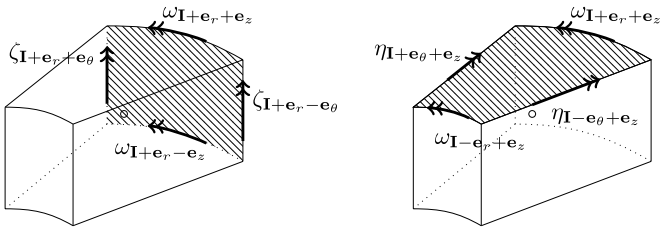

(a) Cell near $r = R$. (b) Cell near $z = L/2$.

Fig. 9. Cells near $r = R$ and $z = L/2$ showing the vorticity components that lie on the (hatched) domain boundaries.

Proof. See Appendix A. □

For finite domains, some care has to be taken for the two inner products to be equal. Investigation of the proof in Appendix A shows that we only have to consider the cells that share a face with the boundary. We assume a finite discretized cylindrical domain of radius R and length L. Arguably the simplest case is when the discrete components of $\boldsymbol{\omega}$ are zero at the boundaries. After inspection of the expressions in Appendix A, this renders the contribution from the cell face at the boundary to both products $(\boldsymbol{\omega}, \overline{\mathbf{C}}\mathbf{u})_{\mathcal{HL}}$ and $(\mathbf{C}\mathbf{u}, \boldsymbol{\omega})_{\mathcal{HS}}$ equal to zero. Subsequently, both inner products only contain the summation of internal values and they are exactly equal.

If the components of $\boldsymbol{\omega}$ are not zero at the wall, then the proof can be used to derive the values for the components of $\mathbf{u}$ in the surrounding layer of ghost cells. Consider a boundary cell with its positive face at $r = R$ which contains two components of $\boldsymbol{\omega}$, namely ω and ζ, and one component of $\mathbf{u}$, namely u_r, as in Fig. 9(a).

From equations (116) and (118), the contributions to the angular component $\omega_{\mathbf{I}+\mathbf{e}_r+\mathbf{e}_z}$ come from cells $\mathbf{I}$ and $\mathbf{I}+2\,\mathbf{e}_z$ alone (since we only sum over internal cells), and together they provide a condition for the value of $u_{z_{\mathbf{I}+2\mathbf{e}_r+\mathbf{e}_z}}$ in the ghost cell layer by solving:

$$\frac{r_{i+\frac{1}{2}}\Delta\theta}{2}\left(\Delta z_k + \Delta z_{k+1}\right) u_{z_{\mathbf{I}+\mathbf{e}_z}} = -\frac{r_{i+\frac{1}{2}}\Delta r_i \Delta\theta}{4}\left(\Delta z_k + \Delta z_{k+1}\right)\frac{2(u_{z_{\mathbf{I}+2\mathbf{e}_r+\mathbf{e}_z}} - u_{z_{\mathbf{I}+\mathbf{e}_z}})}{\Delta r_i + \Delta r_{i+1}}, \tag{50}$$

which yields:

$$u_{z_{\mathbf{I}+2\mathbf{e}_r+\mathbf{e}_z}} = -\frac{\Delta r_{i+1}}{\Delta r_i} u_{z_{\mathbf{I}+\mathbf{e}_z}}, \quad i = N_r. \tag{51}$$

Similarly, from equations (120) and (122), we obtain that the only contributions to the axial component $\zeta_{\mathbf{I}+\mathbf{e}_r+\mathbf{e}_\theta}$ come from cells $\mathbf{I}$ and $\mathbf{I}+2\mathbf{e}_\theta$. Equating yields for the angular velocity $u_{\theta_{\mathbf{I}+2\,\mathbf{e}_r+\mathbf{e}_\theta}}$ in the ghost cell layer:

$$u_{\theta_{\mathbf{I}+2\mathbf{e}_r+\mathbf{e}_\theta}} = -\frac{r_i}{r_{i+1}}\frac{\Delta r_{i+1}}{\Delta r_i} u_{\theta_{\mathbf{I}+\mathbf{e}_\theta}}, \quad i = N_r. \tag{52}$$

The same can be done for the boundaries at $z = \pm L/2$ of the cylindrical grid. There we have the components η and ω of $\boldsymbol{\omega}$ (see Fig. 9(b)). Collecting terms yields for the velocities in the lower ghost value layer:

$$u_{r_{\mathbf{I}+\mathbf{e}_r-2\mathbf{e}_z}} = -\frac{\Delta z_{k-1}}{\Delta z_k} u_{r_{\mathbf{I}+\mathbf{e}_r}}, \quad u_{\theta_{\mathbf{I}+\mathbf{e}_\theta-2\mathbf{e}_z}} = -\frac{\Delta z_{k-1}}{\Delta z_k} u_{\theta_{\mathbf{I}+\mathbf{e}_\theta}}, \quad k = 1, \tag{53}$$

and for the velocities in the upper ghost value layer:

$$u_{r_{\mathbf{I}+\mathbf{e}_r+2\mathbf{e}_z}} = -\frac{\Delta z_{k+1}}{\Delta z_k} u_{r_{\mathbf{I}+\mathbf{e}_r}}, \quad u_{\theta_{\mathbf{I}+\mathbf{e}_\theta+2\mathbf{e}_z}} = -\frac{\Delta z_{k+1}}{\Delta z_k} u_{\theta_{\mathbf{I}+\mathbf{e}_\theta}}, \quad k = N_z. \tag{54}$$

Hence, equality of the inner products can be attained by either choosing the components of the vector $\boldsymbol{\omega}$ in $\mathcal{HL}$ to be zero, or, for non-zero components of $\boldsymbol{\omega}$, the boundary values of the vector $\mathbf{u}$ need to be chosen according to expressions (51)–(54). In section 4.2, we will show that when $\boldsymbol{\omega} = \boldsymbol{\omega}(\mathbf{u})$, these conditions have actual physical meaning: they represent the free-slip (or stress-free) and no-slip boundary conditions for the flow velocity respectively.

3. Mimetic discretization of the Navier–Stokes equations

In this section, we will apply the mimetic discretization techniques from section 2 to generate a finite difference discretization of the incompressible Navier–Stokes equations. We will propose spatial discretizations for the convective part and the viscous part in the next sections. The discretization of the pressure gradient ∇p follows rather trivially: because the pressure is an element of the space HC, the approximation of its gradient is $\overline{\mathbf{G}}p$, with $\overline{\mathbf{G}} : HC \rightarrow \mathcal{HS}$ the adjoint gradient operator as in equations (40)–(42).

3.1. Discretization of the convective term

The convective term of the vector momentum equations $(\mathbf{u}\cdot\nabla)\mathbf{u}$ is a second order tensor, and it does not allow direct application of the mimetic operators derived in section 2. Instead, it can be rewritten as:

$$(\mathbf{u}\cdot\nabla)\mathbf{u} = (\nabla\times\mathbf{u})\times\mathbf{u} + \frac{1}{2}\nabla(\mathbf{u}\cdot\mathbf{u}), \tag{55}$$

occasionally referred to as the rotational formulation, where the right-hand side only consists of first order operators. The term $\frac{1}{2}\nabla(\mathbf{u}\cdot\mathbf{u})$ is added to the pressure gradient, which leaves the term $\mathbf{N}(\mathbf{u}) := (\nabla\times\mathbf{u})\times\mathbf{u} = \boldsymbol{\omega}\times\mathbf{u}$, where $\boldsymbol{\omega}$ is the flow vorticity, as the remaining convection part. With the vorticity in cylindrical coordinates given by:

$$\nabla\times\mathbf{u} = \begin{pmatrix}\eta\\ \omega\\ \zeta\end{pmatrix} = \begin{pmatrix}\frac{1}{r}\frac{\partial u_z}{\partial\theta} - \frac{\partial u_\theta}{\partial z}\\ \frac{\partial u_r}{\partial z} - \frac{\partial u_z}{\partial r}\\ \frac{1}{r}\frac{\partial(r u_\theta)}{\partial r} - \frac{1}{r}\frac{\partial u_r}{\partial\theta}\end{pmatrix}, \tag{56}$$

the convective part $\mathbf{N}$ becomes:

$$\mathbf{N}(\mathbf{u}) = \begin{pmatrix}\omega u_z - \zeta u_\theta\\ \zeta u_r - \eta u_z\\ \eta u_\theta - \omega u_r\end{pmatrix}. \tag{57}$$

The discretization of $\mathbf{N}$ requires the approximation of the vorticity components and subsequently an averaging procedure of the velocity components, as velocity and vorticity are members of different discrete spaces ($\mathcal{HS}$ and $\mathcal{HL}$, respectively). As the velocity vector in the staggered grid is an element of $\mathcal{HS}$, we notice that $\boldsymbol{\omega} = \nabla\times\mathbf{u}$ is discretely approximated by $\overline{\mathbf{C}}\mathbf{u}$, where $\overline{\mathbf{C}}$ is the adjoint curl operator $\overline{\mathbf{C}} : \mathcal{HS}\rightarrow\mathcal{HL}$. Then, with the vorticity components known, the discrete approximation of equation (57) requires spatial averaging to obtain an estimate at the location of the velocity components. The choice of averaging is restricted by the following considerations:

- The averaging should be sufficiently accurate.
- The averaging should be consistent for the cells near the polar axis.
- The averaging should allow conservation of momentum when subjected to discrete integration.
- The averaging should allow conservation of energy in combination with a discrete inner product.

With this in mind, we propose the following discretization for the radial convective part:

$$\begin{aligned}\mathbf{N}_{r_{\mathbf{I}+\mathbf{e}_r}} = {}& \frac{1}{2(\Delta r_i + \Delta r_{i+1})}\left[\omega_{\mathbf{I}+\mathbf{e}_r-\mathbf{e}_z}\left(\Delta r_i u_{z_{\mathbf{I}-\mathbf{e}_z}} + \Delta r_{i+1} u_{z_{\mathbf{I}+2\mathbf{e}_r-\mathbf{e}_z}}\right) + \omega_{\mathbf{I}+\mathbf{e}_r+\mathbf{e}_z}\left(\Delta r_i u_{z_{\mathbf{I}+\mathbf{e}_z}} + \Delta r_{i+1} u_{z_{\mathbf{I}+2\mathbf{e}_r+\mathbf{e}_z}}\right)\right]\\ & - \frac{1}{4}\frac{r_i + r_{i+1}}{2}\left[\zeta_{\mathbf{I}+\mathbf{e}_r-\mathbf{e}_\theta}\left(\frac{u_{\theta_{\mathbf{I}-\mathbf{e}_\theta}}}{r_i} + \frac{u_{\theta_{\mathbf{I}+2\mathbf{e}_r-\mathbf{e}_\theta}}}{r_{i+1}}\right) + \zeta_{\mathbf{I}+\mathbf{e}_r+\mathbf{e}_\theta}\left(\frac{u_{\theta_{\mathbf{I}+\mathbf{e}_\theta}}}{r_i} + \frac{u_{\theta_{\mathbf{I}+2\mathbf{e}_r+\mathbf{e}_\theta}}}{r_{i+1}}\right)\right].\end{aligned} \tag{58}$$

For the angular convective part:

$$\begin{aligned}\mathbf{N}_{\theta_{\mathbf{I}+\mathbf{e}_\theta}} = {}& \frac{1}{2r_i^2\Delta r_i}\left(r_{i-\frac{1}{2}}\frac{r_{i-1}+r_i}{2}\frac{\Delta r_{i-1}+\Delta r_i}{2}\zeta_{\mathbf{I}-\mathbf{e}_r+\mathbf{e}_\theta}\frac{u_{r_{\mathbf{I}-\mathbf{e}_r}} + u_{r_{\mathbf{I}-\mathbf{e}_r+2\mathbf{e}_\theta}}}{2}\right.\\ & \left. + r_{i+\frac{1}{2}}\frac{r_i+r_{i+1}}{2}\frac{\Delta r_i+\Delta r_{i+1}}{2}\zeta_{\mathbf{I}+\mathbf{e}_r+\mathbf{e}_\theta}\frac{u_{r_{\mathbf{I}+\mathbf{e}_r}} + u_{r_{\mathbf{I}+\mathbf{e}_r+2\mathbf{e}_\theta}}}{2}\right)\\ & - \frac{1}{2}\left(\eta_{\mathbf{I}+\mathbf{e}_\theta-\mathbf{e}_z}\frac{u_{z_{\mathbf{I}-\mathbf{e}_z}} + u_{z_{\mathbf{I}+2\mathbf{e}_\theta-\mathbf{e}_z}}}{2} + \eta_{\mathbf{I}+\mathbf{e}_\theta+\mathbf{e}_z}\frac{u_{z_{\mathbf{I}+\mathbf{e}_z}} + u_{z_{\mathbf{I}+2\mathbf{e}_\theta+\mathbf{e}_z}}}{2}\right).\end{aligned} \tag{59}$$

Finally, for the axial convective part:

$$\mathbf{N}_{z_{\mathbf{I}+\mathbf{e}_z}} = \frac{1}{2}\left(\eta_{\mathbf{I}-\mathbf{e}_\theta+\mathbf{e}_z}\frac{\Delta z_k u_{\theta_{\mathbf{I}-\mathbf{e}_\theta}} + \Delta z_{k+1} u_{\theta_{\mathbf{I}-\mathbf{e}_\theta+2\,\mathbf{e}_z}}}{\Delta z_k + \Delta z_{k+1}} + \eta_{\mathbf{I}+\mathbf{e}_\theta+\mathbf{e}_z}\frac{\Delta z_k u_{\theta_{\mathbf{I}+\mathbf{e}_\theta}} + \Delta z_{k+1} u_{\theta_{\mathbf{I}+\mathbf{e}_\theta+2\,\mathbf{e}_z}}}{\Delta z_k + \Delta z_{k+1}}\right)$$
$$- \frac{1}{2r_i}\left(r_{i-\frac{1}{2}}\omega_{\mathbf{I}-\mathbf{e}_r+\mathbf{e}_z}\frac{\Delta z_k u_{r_{\mathbf{I}-\mathbf{e}_r}} + \Delta z_{k+1} u_{r_{\mathbf{I}-\mathbf{e}_r+2\mathbf{e}_z}}}{\Delta z_k + \Delta z_{k+1}} + r_{i+\frac{1}{2}}\omega_{\mathbf{I}+\mathbf{e}_r+\mathbf{e}_z}\frac{\Delta z_k u_{r_{\mathbf{I}+\mathbf{e}_r}} + \Delta z_{k+1} u_{r_{\mathbf{I}+\mathbf{e}_r+2\mathbf{e}_z}}}{\Delta z_k + \Delta z_{k+1}}\right). \tag{60}$$

In section 4 we will show that this choice of discretization leads to conservation of momentum as well as conservation of kinetic energy in the absence of viscosity. In section 5 we will investigate its accuracy.

For comparison with the discretization suggested by Barbosa and Daube [2], the expressions (58)–(60) for uniform grids reduce to:

$$\mathbf{N}_{r_{\mathbf{I}+\mathbf{e}_r}} = \frac{1}{2}\left(\omega_{\mathbf{I}+\mathbf{e}_r-\mathbf{e}_z}\frac{u_{z_{\mathbf{I}-\mathbf{e}_z}} + u_{z_{\mathbf{I}+2\mathbf{e}_r-\mathbf{e}_z}}}{2} + \omega_{\mathbf{I}+\mathbf{e}_r+\mathbf{e}_z}\frac{u_{z_{\mathbf{I}+\mathbf{e}_z}} + u_{z_{\mathbf{I}+2\mathbf{e}_r+\mathbf{e}_z}}}{2}\right)$$
$$- \frac{r_{i+\frac{1}{2}}}{4}\left[\zeta_{\mathbf{I}+\mathbf{e}_r-\mathbf{e}_\theta}\left(\frac{u_{\theta_{\mathbf{I}-\mathbf{e}_\theta}}}{r_i} + \frac{u_{\theta_{\mathbf{I}+2\mathbf{e}_r-\mathbf{e}_\theta}}}{r_{i+1}}\right) + \zeta_{\mathbf{I}+\mathbf{e}_r+\mathbf{e}_\theta}\left(\frac{u_{\theta_{\mathbf{I}+\mathbf{e}_\theta}}}{r_i} + \frac{u_{\theta_{\mathbf{I}+2\mathbf{e}_r+\mathbf{e}_\theta}}}{r_{i+1}}\right)\right], \tag{61}$$

$$\mathbf{N}_{\theta_{\mathbf{I}+\mathbf{e}_\theta}} = \frac{1}{2r_i^2}\left(r_{i-\frac{1}{2}}^2\zeta_{\mathbf{I}-\mathbf{e}_r+\mathbf{e}_r}\frac{u_{r_{\mathbf{I}-\mathbf{e}_r}} + u_{r_{\mathbf{I}-\mathbf{e}_r+2\mathbf{e}_\theta}}}{2} + r_{i+\frac{1}{2}}^2\zeta_{\mathbf{I}+\mathbf{e}_r+\mathbf{e}_\theta}\frac{u_{r_{\mathbf{I}+\mathbf{e}_r}} + u_{r_{\mathbf{I}+\mathbf{e}_r+2\mathbf{e}_\theta}}}{2}\right)$$
$$- \frac{1}{2}\left(\eta_{\mathbf{I}+\mathbf{e}_\theta-\mathbf{e}_z}\frac{u_{z_{\mathbf{I}-\mathbf{e}_z}} + u_{z_{\mathbf{I}+2\mathbf{e}_\theta-\mathbf{e}_z}}}{2} + \eta_{\mathbf{I}+\mathbf{e}_\theta+\mathbf{e}_z}\frac{u_{z_{\mathbf{I}+\mathbf{e}_z}} + u_{z_{\mathbf{I}+2\mathbf{e}_\theta+\mathbf{e}_z}}}{2}\right), \tag{62}$$

$$\mathbf{N}_{z_{\mathbf{I}+\mathbf{e}_z}} = \frac{1}{2}\left(\eta_{\mathbf{I}-\mathbf{e}_\theta+\mathbf{e}_z}\frac{u_{\theta_{\mathbf{I}-\mathbf{e}_\theta}} + u_{\theta_{\mathbf{I}-\mathbf{e}_\theta+2\mathbf{e}_z}}}{2} + \eta_{\mathbf{I}+\mathbf{e}_\theta+\mathbf{e}_z}\frac{u_{\theta_{\mathbf{I}+\mathbf{e}_\theta}} + u_{\theta_{\mathbf{I}+\mathbf{e}_\theta+2\mathbf{e}_z}}}{2}\right)$$
$$- \frac{1}{2r_i}\left(r_{i-\frac{1}{2}}\omega_{\mathbf{I}-\mathbf{e}_r+\mathbf{e}_z}\frac{u_{r_{\mathbf{I}-\mathbf{e}_r}} + u_{r_{\mathbf{I}-\mathbf{e}_r+2\mathbf{e}_z}}}{2} + r_{i+\frac{1}{2}}\omega_{\mathbf{I}+\mathbf{e}_r+\mathbf{e}_z}\frac{u_{r_{\mathbf{I}+\mathbf{e}_r}} + u_{r_{\mathbf{I}+\mathbf{e}_r+2\mathbf{e}_z}}}{2}\right). \tag{63}$$

Although there are global similarities, our radial averaging is quite different. The discretization of Barbosa and Daube [2] seems to require the radial velocity u_r at $r = 0$ for $\mathbf{N}_{\theta_{1,j+\frac{1}{2},k}}$ and the angular vorticity component ω at $r = 0$ for $\mathbf{N}_{z_{1,j,k+\frac{1}{2}}}$, both of which are not defined there. In our discretization, these evaluations at $r = 0$ are resolved using weighted averaging that results in multiplication with the radial coordinate r. Hence, at $r = 0$, any finite value can be assigned to these components as the resulting product always yields zero.

To demonstrate the improvement of the proposed scheme over the scheme of Barbosa and Daube [2], and in particular to emphasize the effect of the different approaches near the origin, two co-rotating vortices of unit circulation are simulated on a disc of radius $R = 8$ m. Their initial radial and angular locations are $(\frac{1}{2}, \pi/10)$ and $(\frac{1}{2}, 11\pi/10)$ respectively. The grid is uniform in all directions for the comparison with 512 and 288 cells in radial and angular direction respectively. The vortices are monitored and Fig. 10 shows their evolution in time for both discretizations in the vicinity of the origin. The results in the left column clearly show the development of a small disturbance around the coordinate origin, while in the right column the contour lines remain smooth. This would suggest that the proposed method leads to more stable and accurate results near the origin.

3.2. Discretization of the viscous term

For constant viscosity flows, the viscous part of the Navier–Stokes equations consists of the vector Laplacian $\nu\Delta\mathbf{u} = \nu\nabla^2\mathbf{u}$, where ν is the kinematic viscosity $\nu = \mu/\rho$. Since the vector Laplacian is a second order operator (divergence of a matrix), the term is rewritten using the identity:

$$\Delta\mathbf{u} = \nabla(\nabla\cdot\mathbf{u}) - \nabla\times\nabla\times\mathbf{u}, \tag{64}$$

which is a mere combination of first order operators. We make the assumption that the first term on the right-hand side of equation (64) can either be neglected in the discretization due to the fact that $\nabla\cdot\mathbf{u} = 0$ is discretely enforced locally in every computational cell, or we add it to the pressure term. This results in the approximation for the viscous part $\mathbf{V}$ as:

$$\mathbf{V}(\mathbf{u}) = -\nu(\nabla\times\nabla\times\mathbf{u}) = -\nu(\nabla\times\boldsymbol{\omega}), \tag{65}$$

where $\boldsymbol{\omega}$ is the flow vorticity as defined in equation (56). The discrete approximation of $\mathbf{V}$ is $\mathbf{C}\overline{\mathbf{C}}\mathbf{u}$, where the discrete curl operators $\overline{\mathbf{C}}: \mathcal{HS}\to\mathcal{HL}$ and $\mathbf{C}: \mathcal{HL}\to\mathcal{HS}$ are used. No averaging is required, and the derivation of both operators in section 2 guarantees that no issues arise for the cells near the polar axis.

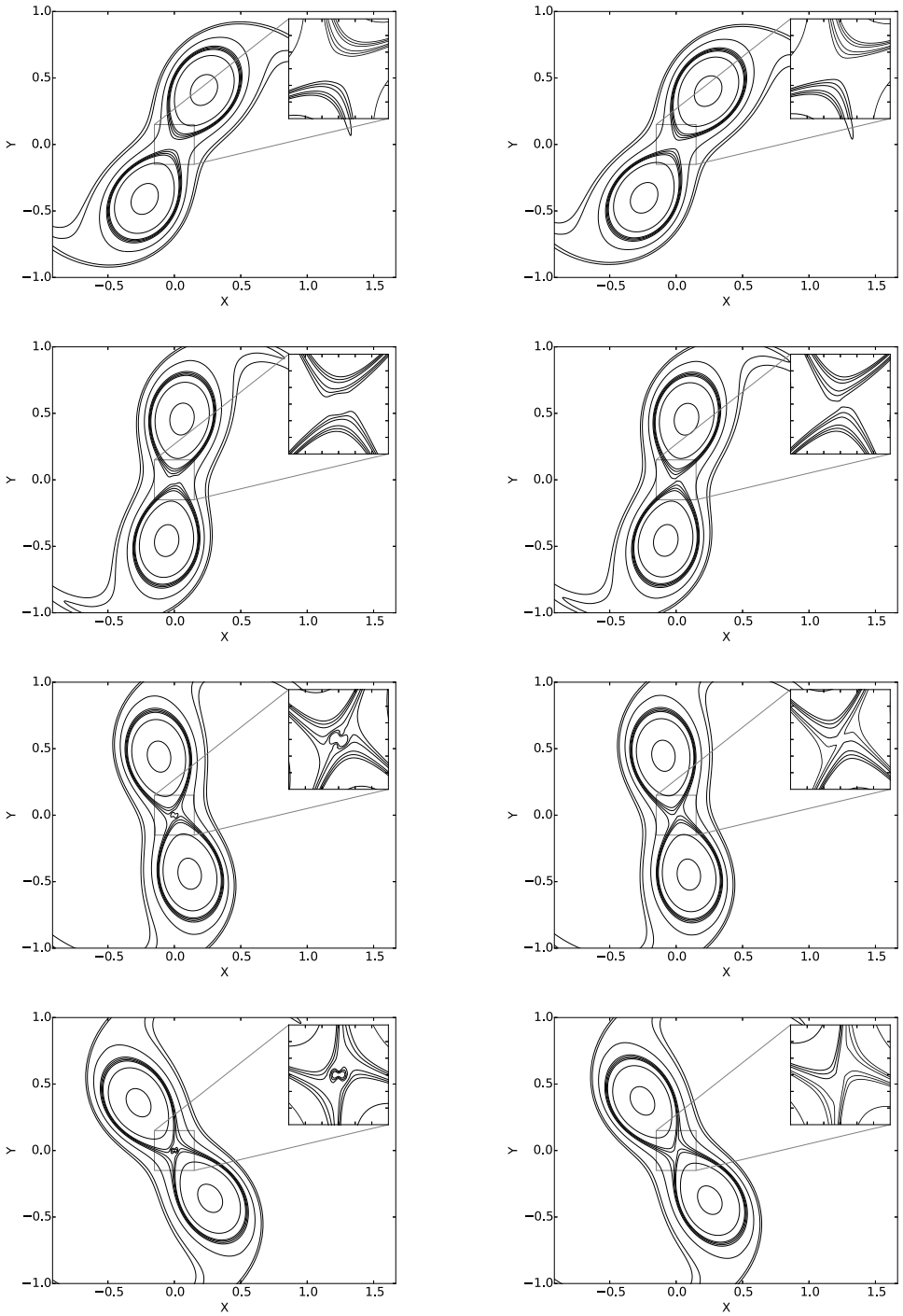

Fig. 10. Evolution (from top to bottom) of the vorticity contours of two co-rotating vortices. The left column displays the results from the discretization of the non-linear terms as in Barbosa and Daube [2], while the right column displays the results from the proposed discretizations (58)–(60). Simulation performed by O. Daube.

3.3. Temporal discretization

The semi-discrete momentum equations and the continuity equation:

$$\frac{\mathrm{d}\mathbf{u}}{\mathrm{d}t} = -\mathbf{N}(\mathbf{u}) - \frac{1}{\rho}\overline{\mathbf{G}}p - \nu\mathbf{C}\overline{\mathbf{C}}\mathbf{u}, \quad \mathbf{D}\mathbf{u} = 0, \qquad \mathbf{u} \in \mathcal{HS},\ p \in HC, \tag{66}$$

are discretized in time using the Implicit Midpoint method:

$$\frac{\mathbf{u}^{(n+1)}-\mathbf{u}^{(n)}}{\Delta t}=-\mathbf{N}\left(\mathbf{u}^{(n+\frac{1}{2})}\right)-\frac{1}{\rho}\overline{\mathbf{G}}p^{(n+\frac{1}{2})}-\nu\mathbf{C}\overline{\mathbf{C}}\mathbf{u}^{(n+\frac{1}{2})},\quad \mathbf{D}\mathbf{u}^{(n+\frac{1}{2})}=0, \tag{67}$$

where $\mathbf{u}^{(n+\frac{1}{2})}=\frac{1}{2}\left(\mathbf{u}^{(n)}+\mathbf{u}^{(n+1)}\right)$. Both the momentum and continuity equations are solved in a coupled way to obtain the solution vector $\left(\mathbf{u}^{(n)},p^{(n)}\right)$ using an iterative Krylov method. In particular, we iterate to obtain the solution of the *non-linear* equations. The Implicit Midpoint method used is second order accurate in time and unconditionally stable (even for vanishing viscosity), which is desirable as the CFL condition becomes very stringent near $r=0$ if explicit methods were to be used. Additionally, if the non-linear coupled equations (67) are solved to machine precision, the method is capable of conserving kinetic energy. We will elaborate on the latter in section 4.3.

4. Conservation properties of the discretization

In this section, we will analyze the conservation properties of the proposed discretization.

4.1. Conservation of mass

The conservation of mass is represented by the discrete continuity equation $\mathbf{D}\mathbf{u}=0$. Since the discrete system is solved in a coupled way, mass conservation is determined by the accuracy of the solution of (67). As iterative methods are often used for this purpose, in practice this implies that the conservation of mass depends on the applied stop criterion of the iterative linear solver.

4.2. Conservation of momentum

Conservation of radial, angular and axial momentum requires the discrete evaluation of:

$$\frac{\mathrm{d}}{\mathrm{d}t}\int_V u_r\,\mathrm{d}V,\quad \frac{\mathrm{d}}{\mathrm{d}t}\int_V ru_\theta\,\mathrm{d}V,\quad \frac{\mathrm{d}}{\mathrm{d}t}\int_V u_z\,\mathrm{d}V, \tag{68}$$

respectively, with V denoting the entire finite cylindrical domain. Proving discrete conservation of momentum has turned out to be complex due to two main reasons. In the first place, looking at the momentum equations (2)–(4), it is clear that the radial and angular momentum equations cannot be trivially written in a conservative formulation, with the time derivative governed solely by flux terms, due to the presence of additional terms that stem from the differentiation of the cylindrical covariant basis vectors which are not constant in space. There exist techniques to rewrite the momentum equations in conservative form (see Vinokur [17]), but they appear to be difficult to integrate into our mimetic approach. A conservative formulation of the governing equations is desirable because it often allows a discrete approximation of a similar form, which in turn leads to discrete conservation almost naturally with only the boundary values contributing. Without conservative formulation, it can be very difficult in practice to obtain conservation numerically, let alone to prove this. The axial momentum equation (4) governing the axial component of the linear momentum fortunately is in conservative form. Furthermore, multiplication of the angular momentum equation (3) with the radial coordinate r yields the conservative formulation for the quantity ru_θ:

$$\frac{\partial(ru_\theta)}{\partial t}+\frac{1}{r}\frac{\partial(r^2u_ru_\theta)}{\partial r}+\frac{1}{r}\frac{\partial(ru_\theta^2)}{\partial\theta}+\frac{\partial(ru_\theta u_z)}{\partial z}=-\frac{1}{\rho r}\frac{\partial(rp)}{\partial\theta}+\frac{1}{\rho r}\frac{\partial(r^2\tau_{r\theta})}{\partial r}+\frac{1}{\rho r}\frac{\partial(r\tau_{\theta\theta})}{\partial\theta}+\frac{1}{\rho}\frac{(r\partial\tau_{\theta z})}{\partial z}, \tag{69}$$

which governs the evolution of the axial component of the angular momentum vector, a conserved quantity in the absence of any external torque applied to the z-axis. For the radial momentum equation, unfortunately, no such procedure seems to exist that converts expression (2) into a conservative formulation. Nonetheless, we will demonstrate that our proposed discretization is capable of conserving radial, angular and axial momentum by numerical validation.

A second difficulty in our approach lies in the rotational formulation of the convective terms. This choice of formulation makes conservation of momentum much less obvious due to the fact that part of the convection is absorbed into an updated pressure variable $\tilde{p}$, which becomes $\tilde{p}=p+\frac{1}{2}\rho\mathbf{u}\cdot\mathbf{u}$. Analytically it holds that:

$$\boldsymbol{\omega}\times\mathbf{u}=\nabla\cdot(\mathbf{u}\mathbf{u})-\mathbf{u}\nabla\cdot\mathbf{u}-\nabla\left(\frac{1}{2}\mathbf{u}\cdot\mathbf{u}\right), \tag{70}$$

where the first term on the right hand side is the conservative formulation and second term involves the flow divergence (and hence vanishes). The third term needs to be balanced by the new pressure $\tilde{p}$, but since this is done implicitly ($\tilde{p}$ is only defined in cell centers), it is impossible to do a term-by-term comparison and therefore to rigorously demonstrate momentum conservation. Equation (70) does however show the dependence of the equality on the flow divergence, and this dependence is observed numerically as well.

For the discrete approximation of the quantities in expression (68), the Trapezoidal rule is used for the spatial integration. This yields the discrete quantities M_r, M_θ and M_z at time $t^{(n)}$ defined as:

$$M_r^{(n)} = \int_V u_r^{(n)}\,\mathrm{d}V \approx \sum_{\mathbf{l}} \frac{\Delta r_i \Delta\theta \Delta z_k}{2}\left(r_{i-\frac{1}{2}} u^{(n)}_{r_{\mathbf{l}-\mathbf{e}_r}} + r_{i+\frac{1}{2}} u^{(n)}_{r_{\mathbf{l}+\mathbf{e}_r}}\right), \tag{71}$$

$$M_\theta^{(n)} = \int_V r u_\theta^{(n)}\,\mathrm{d}V \approx \sum_{\mathbf{l}} \frac{r_i^2 \Delta r_i \Delta\theta \Delta z_k}{2}\left(u^{(n)}_{\theta_{\mathbf{l}-\mathbf{e}_\theta}} + u^{(n)}_{\theta_{\mathbf{l}+\mathbf{e}_\theta}}\right), \tag{72}$$

$$M_z^{(n)} = \int_V u_z^{(n)}\,\mathrm{d}V \approx \sum_{\mathbf{l}} \frac{r_i \Delta r_i \Delta\theta \Delta z_k}{2}\left(u^{(n)}_{z_{\mathbf{l}-\mathbf{e}_z}} + u^{(n)}_{z_{\mathbf{l}+\mathbf{e}_z}}\right). \tag{73}$$

We monitor the values of M_r, M_θ and M_z at every time step, and discrete conservation implies that $M_\alpha^{(n)} = M_\alpha^{(0)}$ for any of the $\alpha \in \{r, \theta, z\}$.

Some attention is required at the boundaries. For our purposes, we will only consider no-slip and free-slip (or stress-free) boundaries. The no-penetration condition $\mathbf{u}\cdot\mathbf{n} = 0$, where $\mathbf{n}$ is the unit normal to the wall, guarantees that the convective parts of the momentum equations do not contribute to any change in momentum. The contribution of the viscous part, which requires boundary conditions for the surrounding layer of ghost cells, is determined by the value of the vorticity at the walls, since:

$$\int_V (\nabla\times\boldsymbol{\omega})\,\mathrm{d}V = \oint_{\partial V} (\mathbf{n}\times\boldsymbol{\omega})\,\mathrm{d}S, \tag{74}$$

where $\mathbf{n}$ is the unit normal to the wall. For free-slip walls, we can enforce the right-hand side of equation (74) to vanish by choosing the discrete velocity boundary conditions in such a way that the resulting vorticity components at the wall are zero. This implies that at the wall $r = R$ both the angular and axial components ω and ζ of the discrete vorticity $\overline{\mathbf{C}}\mathbf{u}$ become zero. From equations (46) and (48), the boundary conditions for the angular and axial velocities then follow as:

$$u_{\theta_{\mathbf{l}+2\mathbf{e}_r+\mathbf{e}_\theta}} = \frac{r_i}{r_{i+1}} u_{\theta_{\mathbf{l}+\mathbf{e}_\theta}} \quad\text{and}\quad u_{z_{\mathbf{l}+2\mathbf{e}_r+\mathbf{e}_z}} = u_{z_{\mathbf{l}+\mathbf{e}_z}}, \quad i = N_r. \tag{75}$$

Notice that during this derivation, the radial velocity u_r is considered to be zero due to the no-penetration condition. At the walls $z = \pm L/2$, the boundary values for the radial and angular velocities follow from equations (44) and (46):

$$u_{r_{\mathbf{l}+\mathbf{e}_r-2\mathbf{e}_z}} = u_{r_{\mathbf{l}+\mathbf{e}_r}} \quad\text{and}\quad u_{\theta_{\mathbf{l}+\mathbf{e}_\theta-2\mathbf{e}_z}} = u_{\theta_{\mathbf{l}+\mathbf{e}_\theta}}, \quad k = 1, \tag{76}$$

$$u_{r_{\mathbf{l}+\mathbf{e}_r+2\mathbf{e}_z}} = u_{r_{\mathbf{l}+\mathbf{e}_r}} \quad\text{and}\quad u_{\theta_{\mathbf{l}+\mathbf{e}_\theta+2\mathbf{e}_z}} = u_{\theta_{\mathbf{l}+\mathbf{e}_\theta}}, \quad k = N_z. \tag{77}$$

In this case, the axial velocity u_z is considered to be zero. Combined, equations (75)–(77) form the free-slip boundary conditions for the velocity, and they follow rather naturally from the construction of the discrete vorticity. Furthermore, with all vorticity components zero at the walls, Proposition 2.2 holds on a finite domain due to the reasoning in section 2.4.

No-slip boundary conditions for finite difference methods are commonly derived by interpolation of the associated velocity to the wall, equating it to zero and subsequently obtaining a value for the velocity component in the ghost cell. We will however proceed along a different path, and derive expressions for the ghost values by instead demanding that Proposition 2.2 remains valid on a finite domain, thereby assuring that the global mimetic structure of the discretization is not impaired. The procedure has in fact already been presented at the end of section 2.4 in the case of non-zero vorticity at the walls. We will repeat the resulting expressions here for completeness: at the wall at $r = R$, it holds that:

$$u_{z_{\mathbf{l}+2\mathbf{e}_r+\mathbf{e}_z}} = -\frac{\Delta r_{i+1}}{\Delta r_i} u_{z_{\mathbf{l}+\mathbf{e}_z}}, \; u_{\theta_{\mathbf{l}+2\mathbf{e}_r+\mathbf{e}_\theta}} = -\frac{r_i}{r_{i+1}}\frac{\Delta r_{i+1}}{\Delta r_i} u_{\theta_{\mathbf{l}+\mathbf{e}_\theta}}, \quad i = N_r, \tag{78}$$

while at the walls at $z = \pm L/2$:

$$u_{r_{\mathbf{l}+\mathbf{e}_r-2\mathbf{e}_z}} = -\frac{\Delta z_{k-1}}{\Delta z_k} u_{r_{\mathbf{l}+\mathbf{e}_r}}, \quad u_{\theta_{\mathbf{l}+\mathbf{e}_\theta-2\mathbf{e}_z}} = -\frac{\Delta z_{k-1}}{\Delta z_k} u_{\theta_{\mathbf{l}+\mathbf{e}_\theta}}, \quad k = 1, \tag{79}$$

$$u_{r_{\mathbf{l}+\mathbf{e}_r+2\mathbf{e}_z}} = -\frac{\Delta z_{k+1}}{\Delta z_k} u_{r_{\mathbf{l}+\mathbf{e}_r}}, \quad u_{\theta_{\mathbf{l}+\mathbf{e}_\theta+2\mathbf{e}_z}} = -\frac{\Delta z_{k+1}}{\Delta z_k} u_{\theta_{\mathbf{l}+\mathbf{e}_\theta}}, \quad k = N_z. \tag{80}$$

Notice that all but the condition for $u_{\theta_{\mathbf{l}+2\,\mathbf{e}_r+\mathbf{e}_\theta}}$ at $r = R$ coincide with the linear interpolation on a non-uniform grid of the velocity component at the wall. The condition for $u_{\theta_{\mathbf{l}+2\mathbf{e}_r+\mathbf{e}_\theta}}$ resembles the linear interpolation of the angular momentum ru_θ instead, and a closer look reveals that it is close to the linear interpolation of u_θ since:

$$u_{\theta_{\mathbf{l}+2\mathbf{e}_r+\mathbf{e}_\theta}} = -\frac{r_i}{r_{i+1}}\frac{\Delta r_{i+1}}{\Delta r_i} u_{\theta_{\mathbf{l}+\mathbf{e}_\theta}} = -\frac{\Delta r_{i+1}}{\Delta r_i}\left(1 - \frac{\Delta r_i + \Delta r_{i+1}}{2r_{i+1}}\right) u_{\theta_{\mathbf{l}+\mathbf{e}_\theta}}, \tag{81}$$

for $i = N_r$. Hence, for sufficiently fine grids it is expected that the conventional linear interpolation of u_θ to the wall is found, but the presence of this extra term must be kept in mind for coarser grids. Finally, equations (78)–(80) constitute the no-slip boundary conditions for the velocity that assure that Proposition 2.2 is valid on a finite domain.

4.3. Conservation of kinetic energy

Summation after taking the inner product of the momentum equations with their respective velocities gives the temporal evolution of the kinetic energy K:

$$\frac{\mathrm{d}K}{\mathrm{d}t} + (\mathbf{N}(\mathbf{u}), \mathbf{u})_{L^2(D)} + \frac{1}{\rho}(\mathbf{G}p, \mathbf{u})_{L^2(D)} - \nu(\mathbf{V}(\mathbf{u}), \mathbf{u})_{L^2(D)} = 0, \tag{82}$$

where $K = (\mathbf{u}, \mathbf{u})_{L^2(D)}/2$ is the L^2-inner product of the velocity vector $\mathbf{u}$ over a suitable domain D, $\mathbf{N}$ is the skew-symmetric convective operator and $\mathbf{V}$ is the symmetric viscous operator. Because $\mathbf{N}$ is skew-symmetric, and with the gradient $\mathbf{G}$ as the formal (negative) adjoint of the divergence $\mathbf{D}$, the second and third terms of equation (82) vanish and the expression reduces to

$$\frac{\mathrm{d}K}{\mathrm{d}t} = \nu(\mathbf{V}(\mathbf{u}), \mathbf{u})_{L^2(D)} = -\nu(\nabla \times \boldsymbol{\omega}, \mathbf{u})_{L^2(D)}. \tag{83}$$

Thus, in the absence of viscosity and with appropriate boundary conditions, the kinetic energy is constant and therefore conserved. We will verify that the proposed discretization satisfies the same conditions, which leads to discrete conservation of kinetic energy as well. The first assumption, $\mathbf{G}$ being the negative adjoint of $\mathbf{D}$, is true by default, as this is precisely how the discrete operator $\mathbf{G}$ was constructed (see section 2). Secondly, it must be shown that the discretization of the convective part does not contribute to the change in kinetic energy.

Proposition 4.1. *The proposed discretization (58)–(60) for the convective part* $\mathbf{N}$ *of the Navier–Stokes equations assures that* $(\mathbf{N}(\mathbf{u}), \mathbf{u})_{\mathcal{HS}} = 0$.

Proof. After performing the inner product (30) over the entire computational domain, we collect all terms that contain the radial component of the vorticity $\eta_{\mathbf{I}+\mathbf{e}_\theta+\mathbf{e}_z}$ for any random choice of $\mathbf{I}$. This comprises the contributions to the inner product from cells $\mathbf{I}$, $\mathbf{I}+2\mathbf{e}_\theta$, $\mathbf{I}+2\mathbf{e}_z$ and $\mathbf{I}+2\mathbf{e}_\theta+2\mathbf{e}_z$. From these four cells, there are angular contributions from $\mathbf{N}_{\theta_{\mathbf{I}+\mathbf{e}_\theta}}$ and $\mathbf{N}_{\theta_{\mathbf{I}+\mathbf{e}_\theta+2\,\mathbf{e}_z}}$ and axial contributions from $\mathbf{N}_{z_{\mathbf{I}+\mathbf{e}_z}}$ and $\mathbf{N}_{z_{\mathbf{I}+2\mathbf{e}_\theta+\mathbf{e}_z}}$, which sum up to:

$$\begin{aligned}
&-C\left(\Delta z_k \overbrace{\frac{u_{z_{\mathbf{I}+\mathbf{e}_z}} + u_{z_{\mathbf{I}+2\mathbf{e}_\theta+\mathbf{e}_z}}}{2}}^{\text{from } \mathbf{N}_{\theta_{\mathbf{I}+\mathbf{e}_\theta}}} u_{\theta_{\mathbf{I}+\mathbf{e}_\theta}} + \Delta z_{k+1} \overbrace{\frac{u_{z_{\mathbf{I}+\mathbf{e}_z}} + u_{z_{\mathbf{I}+2\mathbf{e}_\theta+\mathbf{e}_z}}}{2}}^{\text{from } \mathbf{N}_{\theta_{\mathbf{I}+\mathbf{e}_\theta+2\,\mathbf{e}_z}}} u_{\theta_{\mathbf{I}+\mathbf{e}_\theta+2\,\mathbf{e}_z}}\right) \\
&+C\left(\Delta z_k + \Delta z_{k+1}\right)\left(\underbrace{\frac{1}{2}\frac{\Delta z_k u_{\theta_{\mathbf{I}+\mathbf{e}_\theta}} + \Delta z_{k+1} u_{\theta_{\mathbf{I}+\mathbf{e}_\theta+2\,\mathbf{e}_z}}}{\Delta z_k + \Delta z_{k+1}}}_{\text{from } \mathbf{N}_{z_{\mathbf{I}+\mathbf{e}_z}}} u_{z_{\mathbf{I}+\mathbf{e}_z}} + \underbrace{\frac{1}{2}\frac{\Delta z_k u_{\theta_{\mathbf{I}+\mathbf{e}_\theta}} + \Delta z_{k+1} u_{\theta_{\mathbf{I}+\mathbf{e}_\theta+2\mathbf{e}_z}}}{\Delta z_k + \Delta z_{k+1}}}_{\text{from } \mathbf{N}_{z_{\mathbf{I}+2\mathbf{e}_\theta+\mathbf{e}_z}}} u_{z_{\mathbf{I}+2\mathbf{e}_\theta+\mathbf{e}_z}}\right),
\end{aligned} \tag{84}$$

where $C = \frac{1}{2} r_i \Delta r_i \Delta\theta$. It can be seen that these terms add up to zero.

Then we collect all terms that contain the angular component of the vorticity $\omega_{\mathbf{I}+\mathbf{e}_r+\mathbf{e}_z}$ for any random $\mathbf{I}$. This comprises the contributions to the inner product from cells $\mathbf{I}$, $\mathbf{I}+2\mathbf{e}_r$, $\mathbf{I}+2\mathbf{e}_z$ and $\mathbf{I}+2\mathbf{e}_r+2\mathbf{e}_z$. From these four cells, there are radial contributions from $\mathbf{N}_{r_{\mathbf{I}+\mathbf{e}_r}}$ and $\mathbf{N}_{r_{\mathbf{I}+\mathbf{e}_r+2\mathbf{e}_z}}$ and axial contributions from $\mathbf{N}_{z_{\mathbf{I}+\mathbf{e}_z}}$ and $\mathbf{N}_{z_{\mathbf{I}+2\mathbf{e}_r+\mathbf{e}_z}}$, which sum up to:

$$\begin{aligned}
&C\left(\Delta r_i + \Delta r_{i+1}\right)\left(\Delta z_k \overbrace{\frac{1}{2}\frac{\Delta r_i u_{z_{\mathbf{I}+\mathbf{e}_z}} + \Delta r_{i+1} u_{z_{\mathbf{I}+2\mathbf{e}_r+\mathbf{e}_z}}}{\Delta r_i + \Delta r_{i+1}}}^{\text{from } \mathbf{N}_{r_{\mathbf{I}+\mathbf{e}_r}}} u_{r_{\mathbf{I}+\mathbf{e}_r}} + \Delta z_{k+1} \overbrace{\frac{1}{2}\frac{\Delta r_i u_{z_{\mathbf{I}+\mathbf{e}_z}} + \Delta r_{i+1} u_{z_{\mathbf{I}+2\mathbf{e}_r+\mathbf{e}_z}}}{\Delta r_i + \Delta r_{i+1}}}^{\text{from } \mathbf{N}_{r_{\mathbf{I}+\mathbf{e}_r+2\mathbf{e}_z}}} u_{r_{\mathbf{I}+\mathbf{e}_r+2\mathbf{e}_z}}\right) \\
&-C\left(\Delta z_k + \Delta z_{k+1}\right)\left(\Delta r_i \underbrace{\frac{1}{2}\frac{\Delta z_k u_{r_{\mathbf{I}+\mathbf{e}_r}} + \Delta z_{k+1} u_{r_{\mathbf{I}+\mathbf{e}_r+2\mathbf{e}_z}}}{\Delta z_k + \Delta z_{k+1}}}_{\text{from } \mathbf{N}_{z_{\mathbf{I}+\mathbf{e}_z}}} u_{z_{\mathbf{I}+\mathbf{e}_z}} + \Delta r_{i+1} \underbrace{\frac{1}{2}\frac{\Delta z_k u_{r_{\mathbf{I}+\mathbf{e}_r}} + \Delta z_{k+1} u_{r_{\mathbf{I}+\mathbf{e}_r+2\mathbf{e}_z}}}{\Delta z_k + \Delta z_{k+1}}}_{\text{from } \mathbf{N}_{z_{\mathbf{I}+2\mathbf{e}_r+\mathbf{e}_z}}} u_{z_{\mathbf{I}+2\mathbf{e}_r+\mathbf{e}_z}}\right),
\end{aligned} \tag{85}$$

with $C = \frac{1}{2} r_{i+\frac{1}{2}} \Delta\theta$. After some algebraic manipulation, it follows that these terms also add up to zero.

Finally, we collect all terms that contain the axial component of the vorticity $\zeta_{\mathbf{I}+\mathbf{e}_r+\mathbf{e}_\theta}$ for any random $\mathbf{I}$, which comprises the contributions to the inner product from cells $\mathbf{I}$, $\mathbf{I}+2\mathbf{e}_r$, $\mathbf{I}+2\mathbf{e}_\theta$ and $\mathbf{I}+2\mathbf{e}_r+2\mathbf{e}_\theta$. From these four cells, there are radial contributions from $\mathbf{N}_{r_{\mathbf{I}+\mathbf{e}_r}}$ and $\mathbf{N}_{r_{\mathbf{I}+\mathbf{e}_r+2\mathbf{e}_\theta}}$ and angular contributions from $\mathbf{N}_{\theta_{\mathbf{I}+\mathbf{e}_\theta}}$ and $\mathbf{N}_{\theta_{\mathbf{I}+2\mathbf{e}_r+\mathbf{e}_\theta}}$, which sum up to

$$
\begin{aligned}
&-\frac{C}{4}\frac{r_i+r_{i+1}}{2}\Bigg[\overbrace{\left(\frac{u_{\theta_{\mathbf{I}+\mathbf{e}_\theta}}}{r_i}+\frac{u_{\theta_{\mathbf{I}+2\mathbf{e}_r+\mathbf{e}_\theta}}}{r_{i+1}}\right)}^{\text{from } \mathbf{N}_{r_{\mathbf{I}+\mathbf{e}_r}}} u_{r_{\mathbf{I}+\mathbf{e}_r}}+\overbrace{\left(\frac{u_{\theta_{\mathbf{I}+\mathbf{e}_\theta}}}{r_i}+\frac{u_{\theta_{\mathbf{I}+2\mathbf{e}_r+\mathbf{e}_\theta}}}{r_{i+1}}\right)}^{\text{from } \mathbf{N}_{r_{\mathbf{I}+\mathbf{e}_r+2\mathbf{e}_\theta}}} u_{r_{\mathbf{I}+\mathbf{e}_r+2\mathbf{e}_\theta}}\Bigg]\\
&+\frac{C}{4}\frac{r_i+r_{i+1}}{2}\Bigg[\underbrace{\frac{u_{r_{\mathbf{I}+\mathbf{e}_r}}+u_{r_{\mathbf{I}+\mathbf{e}_r+2\mathbf{e}_\theta}}}{r_i}}_{\text{from } \mathbf{N}_{\theta_{\mathbf{I}+\mathbf{e}_\theta}}} u_{\theta_{\mathbf{I}+\mathbf{e}_\theta}}+\underbrace{\frac{u_{r_{\mathbf{I}+\mathbf{e}_r}}+u_{r_{\mathbf{I}+\mathbf{e}_r+2\mathbf{e}_\theta}}}{r_{i+1}}}_{\text{from } \mathbf{N}_{\theta_{\mathbf{I}+2\mathbf{e}_r+\mathbf{e}_\theta}}} u_{\theta_{\mathbf{I}+2\mathbf{e}_r+\mathbf{e}_\theta}}\Bigg],
\end{aligned}
\tag{86}
$$

with $C=\frac{1}{2}r_{i+\frac{1}{2}}(\Delta r_i+\Delta r_{i+1})\Delta\theta\Delta z_k$. It can be seen that these terms sum up to zero as well. Since this holds for all elements of the vorticity vector, the inner product yields exactly zero. □

The Implicit Midpoint time integration method applied to the semi-discrete Navier–Stokes without viscosity or external forces gives:

$$
\frac{\mathbf{u}^{(n+1)}-\mathbf{u}^{(n)}}{\Delta t}=-\mathbf{N}\left(\mathbf{u}^{(n+\frac{1}{2})}\right)-\overline{\mathbf{G}}p^{(n+\frac{1}{2})},\qquad \mathbf{D}\mathbf{u}^{(n+\frac{1}{2})}=0,
\tag{87}
$$

with $\mathbf{u}^{(n+\frac{1}{2})}=\frac{1}{2}(\mathbf{u}^{(n)}+\mathbf{u}^{(n+\frac{1}{2})})$. Notice that the inner product of the left-hand side of equation (87) with $\mathbf{u}^{(n+\frac{1}{2})}$ yields:

$$
\left(\frac{\mathbf{u}^{(n+1)}-\mathbf{u}^{(n)}}{\Delta t},\mathbf{u}^{(n+\frac{1}{2})}\right)_{\mathcal{HS}}=\frac{1}{2\Delta t}\left[\left(\mathbf{u}^{(n+1)},\mathbf{u}^{(n+1)}\right)_{\mathcal{HS}}-\left(\mathbf{u}^{(n)},\mathbf{u}^{(n)}\right)_{\mathcal{HS}}\right],
\tag{88}
$$

while taking the inner product with the right-hand side gives:

$$
-\left(\mathbf{N}(\mathbf{u}^{(n+\frac{1}{2})}),\mathbf{u}^{(n+\frac{1}{2})}\right)_{\mathcal{HS}}-\left(\overline{\mathbf{G}}p^{(n+\frac{1}{2})},\mathbf{u}^{(n+\frac{1}{2})}\right)_{\mathcal{HS}}=\left(p^{(n+\frac{1}{2})},\mathbf{D}\mathbf{u}^{(n+\frac{1}{2})}\right)_{HN}
\tag{89}
$$

by Proposition 4.1 and the definition of the gradient operator $\overline{\mathbf{G}}$. Combining equations (88) and (89) then shows that:

$$
\left(\mathbf{u}^{(n+1)},\mathbf{u}^{(n+1)}\right)_{\mathcal{HS}}-\left(\mathbf{u}^{(n)},\mathbf{u}^{(n)}\right)_{\mathcal{HS}}=2\Delta t\left(p^{(n+\frac{1}{2})},\mathbf{D}\mathbf{u}^{(n+\frac{1}{2})}\right)_{HN}.
\tag{90}
$$

If we define the kinetic energy at time t^n as $K^{(n)}:=\frac{1}{2}\left(\mathbf{u}^{(n)},\mathbf{u}^{(n)}\right)_{\mathcal{HS}}$, then

$$
\frac{K^{(n+1)}-K^{(n)}}{\Delta t}=\left(p^{(n+\frac{1}{2})},\mathbf{D}\mathbf{u}^{(n+\frac{1}{2})}\right)_{HN},
\tag{91}
$$

and conservation of kinetic energy depends solely on the value of $\mathbf{D}\mathbf{u}$ in the domain. Hence, for vanishing flow divergence $\mathbf{D}\mathbf{u}=0$, it follows that the discrete kinetic energy is conserved.

For viscous flows, it is well known that the temporal decay of kinetic energy due to viscous dissipation on a suitable domain is given by

$$
\frac{\mathrm{d}K}{\mathrm{d}t}=-2\nu\mathcal{E},
\tag{92}
$$

where $\mathcal{E}=\frac{1}{2}\int_V|\nabla\times\mathbf{u}|^2\,\mathrm{d}V$ is the flow enstrophy. Notice that this expression follows from applying the self-adjointness of the curl operator to the right-hand side of equation (83). At the discrete level, the fully discretized momentum equations without external forces read:

$$
\frac{\mathbf{u}^{(n+1)}-\mathbf{u}^{(n)}}{\Delta t}=-\mathbf{N}\left(\mathbf{u}^{(n+\frac{1}{2})}\right)-\overline{\mathbf{G}}p^{(n+\frac{1}{2})}-\nu\mathbf{C}\overline{\mathbf{C}}\mathbf{u}^{(n+\frac{1}{2})}.
\tag{93}
$$

Taking the inner product with $\mathbf{u}^{(n+\frac{1}{2})}$ once more now yields:

$$
\frac{K^{(n+1)}-K^{(n)}}{\Delta t}=-\nu\left(\mathbf{C}\overline{\mathbf{C}}\mathbf{u}^{(n+\frac{1}{2})},\mathbf{u}^{(n+\frac{1}{2})}\right)_{\mathcal{HS}},
\tag{94}
$$

where we have used the fact that the convective term does not contribute to the evolution of the kinetic energy, and the pressure term vanishes because $\mathbf{D}\mathbf{u}=0$ as noted above. By Proposition 2.2, the term on the right-hand side is equal to

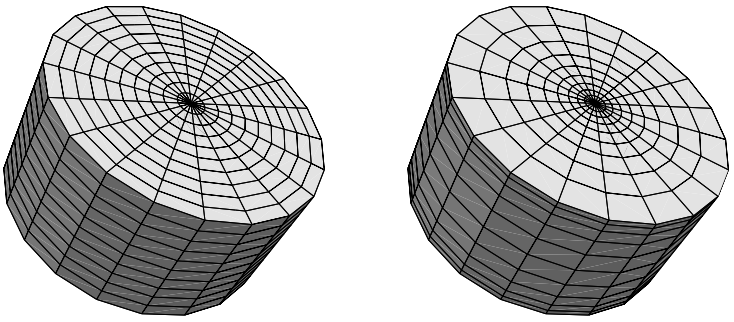

(a) Uniform distribution. (b) Non-uniform distribution.

Fig. 11. The uniform and non-uniform node distributions.

$$\nu\left(\mathbf{C}\overline{\mathbf{C}}\mathbf{u}^{(n+\frac{1}{2})},\mathbf{u}^{(n+\frac{1}{2})}\right)_{\mathcal{HS}}=\nu\left(\overline{\mathbf{C}}\mathbf{u}^{(n+\frac{1}{2})},\overline{\mathbf{C}}\mathbf{u}^{(n+\frac{1}{2})}\right)_{\mathcal{HL}}, \tag{95}$$

which is the discrete representation of twice the enstrophy. Hence, with the flow divergence **Du** equal to zero, the resulting expression:

$$\frac{K^{(n+1)}-K^{(n)}}{\Delta t}=-2\nu\left(\overline{\mathbf{C}}\mathbf{u}^{(n+\frac{1}{2})},\overline{\mathbf{C}}\mathbf{u}^{(n+\frac{1}{2})}\right)_{\mathcal{HL}}, \tag{96}$$

is the discrete analogue of expression (92).

5. Numerical validation

In this section, we will numerically demonstrate the conservation properties of the proposed discretization on both uniform and non-uniform grids (section 5.1). Furthermore, we will demonstrate the formal accuracy of the proposed method (section 5.2). For this, we use the Method of Manufactured Solutions, which we believe is among the most rigorous procedures to determine the general numerical accuracy.

5.1. Conservation properties

We are interested in the temporal evolution of mass, momentum and kinetic energy (in absence of viscosity). In sections 4.1 and 4.2 it was observed that conservation of mass and momentum are both determined by the accuracy of the solution of the continuity equation $\mathbf{Du}=0$. In our simulations, we therefore set the stopping criterion for the iterative linear solver (based on the relative residual) to 10^{-15} to enforce conservation of mass and momentum up to machine precision. To investigate the energy conservation capacity of the discretization, we consider a flow in a cylinder of radius 1 m and length 1 m. The velocities are initialized as random numbers from the interval $[-\frac{1}{2},\frac{1}{2}]$, and subsequently the flow field is made divergence-free by a projection step, where the initial pressure is also calculated. On the solid walls at $r=R$ and $z=\pm\frac{L}{2}$, a free-slip or stress-free boundary condition is imposed as described by equations (75)–(77). The free-slip condition assures that the vorticity at the wall is zero and therefore it does not contribute to any change in momentum. The fluid viscosity is set to zero, and we perform the simulation up to time $T=10$ seconds, while observing the discrete mass, momentum and kinetic energy at every time step. A small time step Δt of 10^{-5} seconds is chosen purely to guarantee convergence of our current non-linear solver, as the conservation properties are independent of the magnitude of the time step. To verify the proposed discretization on grids with non-uniform node distributions, the simulations are performed on two grids: a uniform grid, where $r_{i+\frac{1}{2}}=(i+\frac{1}{2})R/N_r$ and $z_{k+\frac{1}{2}}=-\frac{L}{2}+(k-\frac{1}{2})L/N_z$, and a grid with a non-uniform distributions defined by

$$r_{i+\frac{1}{2}}=R\left(\frac{e^{\alpha i R/N_r}-1}{e^{\alpha R}-1}\right),\qquad i=0,\ldots,N_r, \tag{97}$$

$$z_{k+\frac{1}{2}}=\frac{L}{2}\frac{\tanh(\beta i/N_z)}{\tanh(\beta L/2)},\qquad k=0,\ldots,N_z, \tag{98}$$

with $\alpha=2$ and $\beta=3$ as depicted in Fig. 11. Although perhaps not very applicable in practice, we have chosen this distribution in particular to demonstrate the validity of our conservation claims in the case of a severe variety in cell size throughout the computational domain. The number of grid cells are $10\times20\times10$ in radial, angular and axial direction respectively.

For the inviscid computations, we also calculate the resulting flow field using the spatial discretization of Morinishi et al. [12] for comparison. Because it is known that their axis treatment may introduce instabilities, we use the averaging procedure of Fukagata and Kasagi [5] for the radial velocity at $r=0$, which does not conserve kinetic energy exactly. We find that the proposed method conserves mass, momentum and kinetic energy up to machine precision, as expected.

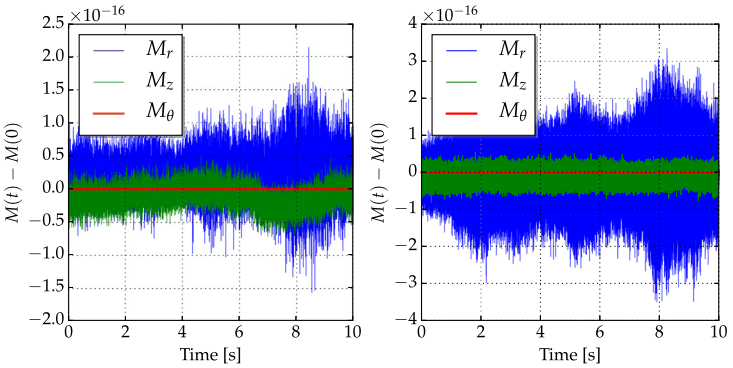

(a) Uniform grid. (b) Non-uniform grid.

Fig. 12. Momentum evolution on both uniform and non-uniform grid.

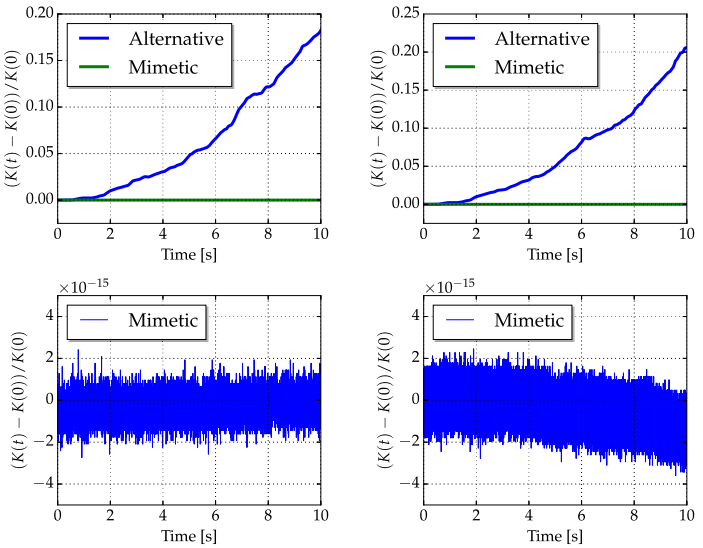

(a) Uniform grid. (b) Non-uniform grid.

Fig. 13. Normalized kinetic energy evolution on both uniform and non-uniform grid. The mimetic results are shown separately in the lower figures for a better impression of the actual magnitude.

Conservation of mass and momentum is obtained for the discretization technique of Morinishi et al. [12] (this is also proven in their paper). However, the kinetic energy is not conserved in time, which is likely due to the handling of the radial velocity at the polar axis. First, Fig. 12 shows the evolution of the discrete radial, angular and axial momenta M_α of equations (71)–(73) using the proposed discretization. On both uniform and non-uniform grids, all three momenta are conserved to machine precision. The radial and axial momenta are of the order of machine precision initially, while the angular momentum maintains a larger non-zero value. Fig. 13 then shows the kinetic energy during the simulation for both methods on the two grid types: the combined method of Morinishi et al. [12] and Fukagata and Kasagi [5] is referred to as the 'alternative' method.

For viscous flows, the kinetic energy decays at a rate determined by the flow enstrophy $\mathcal{E}$ as defined in section 4.3. To test this, we simulate a swirling flow with an angular velocity $u_\theta(r) = R(r - r^2)$. No-slip boundary conditions are applied for the velocity, and the dynamic viscosity has a value of $\mu = 0.01$ kg/m/s. Both the kinetic energy and the flow enstrophy are monitored in time. Fig. 14 shows the monotone decay of the kinetic energy in time for both uniform and non-uniform grids based on the proposed discretization. We have used three levels of refinement to demonstrate that the uniform and non-uniform results converge to the same rate of energy decay. As a consistency check, we have compared the energy decay in time at semi-integer time levels by explicitly calculating both sides of equation (96), i.e. the time derivative of the kinetic energy:

$$\frac{\mathrm{d}K}{\mathrm{d}t}(t^{n+\frac{1}{2}}) \approx \frac{K^{(n+1)} - K^{(n)}}{\Delta t}, \tag{99}$$

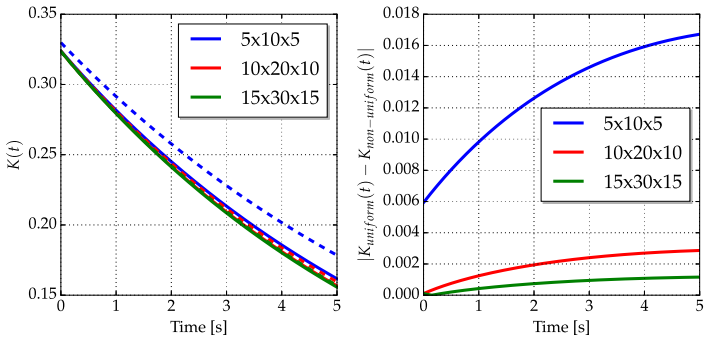

Fig. 14. Kinetic energy decay for a viscous flow for different levels of grid refinement, and the error between the results on uniform (solid line) and non-uniform (hatched line) grids.

and the scaled flow enstrophy, calculated as:

$$-2\nu\mathcal{E}(t^{n+\frac{1}{2}}) \approx -2\nu\left(\overline{\mathbf{C}}\mathbf{u}^{(n+\frac{1}{2})}, \overline{\mathbf{C}}\mathbf{u}^{(n+\frac{1}{2})}\right)_{\mathcal{HL}}. \tag{100}$$

For the proposed approach, we find that the difference of the two terms is in the order of machine precision for both the uniform and the non-uniform grid.

5.2. Spatial accuracy

In order to demonstrate the formal accuracy of the proposed discretization, we utilize the Method of Manufactured Solutions (MMS) [13]. With a properly chosen solution, the MMS is capable of testing virtually all terms of the discretization, and, if necessary, even individually. This is generally more challenging than comparison with known exact solutions, which, if they exist in closed form at all, often follow from applying highly simplifying assumptions and therefore they may not involve all the terms in the Navier–Stokes equations.

One of the recommended properties of manufactured solutions is that they are sufficiently smooth, so that they do not prevent the theoretical order of accuracy being obtained. Therefore, we choose the following time-dependent solutions for the velocity components and the pressure:

$$u_r(r,\theta,z,t) = (r-R)\left(z-\frac{L}{2}\right)\left(z+\frac{L}{2}\right)\cos(rz)\sin(\theta)\sin(t), \tag{101}$$

$$u_\theta(r,\theta,z,t) = (r-R)\left(z-\frac{L}{2}\right)\left(z+\frac{L}{2}\right)\sin(r+\theta+z)\sin(t), \tag{102}$$

$$u_z(r,\theta,z,t) = (r-R)\left(z-\frac{L}{2}\right)\left(z+\frac{L}{2}\right)\cos(r\theta z)\sin(t), \tag{103}$$

$$p(r,\theta,z,t) = \cos\left(\frac{2\pi r}{R}\right)\cos\left(\frac{2\pi\left(z+\frac{L}{2}\right)}{L}\right)\sin(t), \tag{104}$$

where $R = 1$ m is the cylinder radius and $L = 1$ m its length. The manufactured velocity solutions satisfy no-slip boundary conditions at the walls, while there is a non-zero radial flow through the origin. The pressure satisfies homogeneous Neumann conditions at all walls. Using a symbolic computer algebra program, the solutions (101)–(104) are inserted in the Navier–Stokes equations (67), and the output is added to the right-hand side of the momentum equations. No-slip boundary conditions are applied, and initially all velocities and the pressure are set to zero. We then perform simulations until a certain time T on four grids with $(5 \times 10 \times 5)$, $(10 \times 20 \times 10)$, $(20 \times 40 \times 20)$ and $(40 \times 80 \times 40)$ cells. Both a uniform and a non-uniform grid as in equations (97) and (98) are used. Since the computations are unsteady, a very small time step of $\Delta t = 10^{-7}$ is chosen to assure that the temporal error is negligible compared to the spatial error. The fixed time step is reduced for each grid refinement in order to keep the Courant number approximately constant. We then

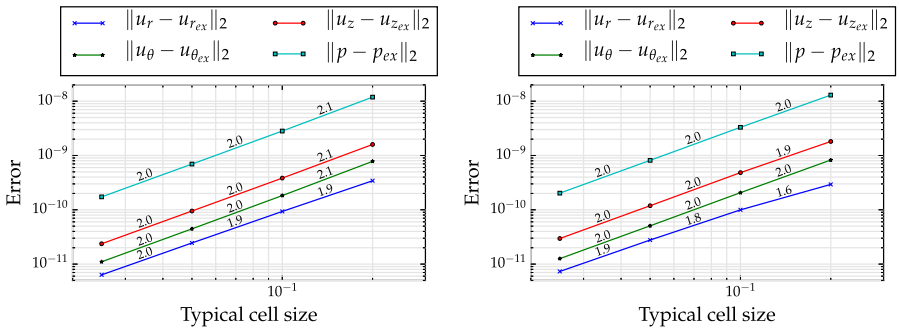

(a) Global error on a uniform grid.

(b) Global error on a non-uniform grid.

Fig. 15. Grid convergence of the proposed discretization using the MMS. For plotting purposes, the pressure error is scaled down by a factor of 10^5.

determine the global error by approximating the discrete L^2-norm at time T for all three velocity components by calculating:

$$\|u - u_{ex}\|_2 = \sqrt{\sum_{i,j,k} \left(u^{(T)}_{i,j,k} - u_{ex}(r_i, \theta_j, z_k, T)\right)^2 r_i \Delta r_i \Delta\theta \Delta z_k}, \tag{105}$$

and

$$\|p - p_{ex}\|_2 = \sqrt{\sum_{i,j,k} \left(p^{(T)}_{i,j,k} - p_{ex}(r_i, \theta_j, z_k, T)\right)^2 r_i \Delta r_i \Delta\theta \Delta z_k}, \tag{106}$$

where $u^{(T)}_{i,j,k}$ and $p^{(T)}_{i,j,k}$ are the calculated solutions for any of the velocity components and the pressure at location (r_i, θ_j, z_k) at time T, u_{ex} and p_{ex} the associated exact solutions value and $r_i \Delta r_i \Delta\theta \Delta z_k$ the volume of the cell (i, j, k). The results for both uniform and non-uniform grids are shown in Fig. 15, where the error against the typical cell size is plotted. For both uniform and non-uniform grids, the global error of all flow variables shows second order behavior as the grid size goes to zero.

6. Concluding remarks

The aim of this paper was to construct a spatial finite difference discretization of the cylindrical Navier–Stokes equations that conserves mass, momentum and kinetic energy, while simultaneously treating the classical problem near and at the origin $r = 0$. We have used the mimetic finite difference method to derive the vector identities like the gradient, the curl and the divergence. We have shown that the proposed averaging procedure is able to conserve mass and momentum and, in the absence of viscosity, also kinetic energy on both uniform and non-uniform grids. The mimetic approach combined with the averaging also yields a natural treatment of the singularity at $r = 0$. Accuracy tests show second order convergence in space on both grids with uniform and non-uniform node distribution.

For large LES or DNS calculations, it is likely that the overall second order accuracy of the proposed method is too restrictive. Therefore, future work should investigate the possibility of higher order approximations while maintaining the conservation properties.

The proposed spatial discretization alone is not sufficient for kinetic energy conservation. The time advancement of the semi-discrete equations is equally important, as any damping present may destroy the inherent conservation properties. In this paper, we have used an implicit method known to conserve quadratic invariants to demonstrate the capabilities of the proposed spatial discretization. Besides being implicit, our approach hinges on the solution of the non-linear equations, which makes the computational procedure even more costly. In practice, both this and an implicit system may be unfeasible for large grids, and other (explicit) methods could be considered that (nearly) conserve energy: Verstappen and Veldman [15] for example propose a class of time integration methods for this purpose. Here the trade-off is clearly between computational cost and the level of the conservation of the method.

Acknowledgements

The authors would like to thank Deltares, TNO and Shell for their financial support during this research. Furthermore, we thank Arthur Veldman for helpful suggestions. Olivier Daube is greatly acknowledged for fruitful discussions and for performing the rotating vortices test case in section 3.1. Finally, we thank the reviewers for their remarks and suggestions that have improved the quality of this manuscript.

Appendix A. Proofs of mimetic inner products

In this appendix, the proofs from section 2.4 are provided.

Proposition. *For any $p \in HC$ and $\mathbf{u} \in \mathcal{HS}$ on an infinite domain, it holds that* $(\mathbf{Du}, p)_{HC} = -(\mathbf{u}, \overline{\mathbf{G}}p)_{\mathcal{HS}}$.

Proof. Let $p \in HC$ and $\mathbf{u} = (u_r, u_\theta, u_z) \in \mathcal{HS}$. We start with the inner product $(\mathbf{Du}, p)_{HC}$. For cell $\mathbf{I}$, this is given by

$$(\mathbf{Du}, p)_{HC_\mathbf{I}} = V_\mathbf{I} \left(\frac{r_{i+\frac{1}{2}} u_{r_{\mathbf{I}+\mathbf{e}_r}} - r_{i-\frac{1}{2}} u_{r_{\mathbf{I}-\mathbf{e}_r}}}{r_i \Delta r_i} + \frac{u_{\theta_{\mathbf{I}+\mathbf{e}_\theta}} - u_{\theta_{\mathbf{I}-\mathbf{e}_\theta}}}{r_i \Delta\theta} + \frac{u_{z_{\mathbf{I}+\mathbf{e}_z}} - u_{z_{\mathbf{I}-\mathbf{e}_z}}}{\Delta z_k} \right) p_\mathbf{I} \tag{107}$$

$$= \left(\Delta\theta \Delta z_k (r_{i+\frac{1}{2}} u_{r_{\mathbf{I}+\mathbf{e}_r}} - r_{i-\frac{1}{2}} u_{r_{\mathbf{I}-\mathbf{e}_r}}) + \Delta r_i \Delta z_k (u_{\theta_{\mathbf{I}+\mathbf{e}_\theta}} - u_{\theta_{\mathbf{I}-\mathbf{e}_\theta}}) + r_i \Delta r_i \Delta\theta (u_{z_{\mathbf{I}+\mathbf{e}_z}} - u_{z_{\mathbf{I}-\mathbf{e}_z}}) \right) p_\mathbf{I} \tag{108}$$

where $V_\mathbf{I} = r_i \Delta r_i \Delta\theta \Delta z_k$ is the volume of cell $\mathbf{I}$. Then, for the inner product $(\mathbf{u}, \overline{\mathbf{G}}p)_{\mathcal{HS}}$, we collect all contributions to an arbitrary $p_\mathbf{I}$. For an arbitrary cell $\mathbf{I}$:

$$\begin{aligned}(\mathbf{u}, \overline{\mathbf{G}}p)_{\mathcal{HS}_\mathbf{I}} = \frac{\Delta r_i \Delta\theta \Delta z_k}{2} \Bigg[& r_{i-\frac{1}{2}} u_{r_{\mathbf{I}-\mathbf{e}_r}} \frac{2(p_\mathbf{I} - p_{\mathbf{I}-2\mathbf{e}_r})}{\Delta r_{i-1} + \Delta r_i} + r_{i+\frac{1}{2}} u_{r_{\mathbf{I}+\mathbf{e}_r}} \frac{2(p_{\mathbf{I}+2\mathbf{e}_r} - p_\mathbf{I})}{\Delta r_i + \Delta r_{i+1}} \\ & + r_i \left(u_{\theta_{\mathbf{I}-\mathbf{e}_\theta}} \frac{p_\mathbf{I} - p_{\mathbf{I}-2\mathbf{e}_\theta}}{r_i \Delta\theta} + u_{\theta_{\mathbf{I}+\mathbf{e}_\theta}} \frac{p_{\mathbf{I}+2\mathbf{e}_\theta} - p_\mathbf{I}}{r_i \Delta\theta} \right) \\ & + r_i \left(u_{z_{\mathbf{I}-\mathbf{e}_z}} \frac{2(p_\mathbf{I} - p_{\mathbf{I}-2\mathbf{e}_z})}{\Delta z_{k-1} + \Delta z_k} + u_{z_{\mathbf{I}+\mathbf{e}_z}} \frac{2(p_{\mathbf{I}+2\mathbf{e}_z} - p_\mathbf{I})}{\Delta z_k + \Delta z_{k+1}} \right) \Bigg].\end{aligned} \tag{109}$$

Collecting all radial contributions to $p_\mathbf{I}$ gives:

$$-\frac{1}{2} \Bigg[\overbrace{-\Delta r_{i-1} \Delta\theta \Delta z_k \left(\frac{2 r_{i-\frac{1}{2}} u_{r_{\mathbf{I}-\mathbf{e}_r}}}{\Delta r_{i-1} + \Delta r_i} \right)}^{\text{from cell } \mathbf{I}-2\mathbf{e}_r} \overbrace{+\Delta r_{i+1} \Delta\theta \Delta z_k \left(\frac{2 r_{i+\frac{1}{2}} u_{r_{\mathbf{I}+\mathbf{e}_r}}}{\Delta r_i + \Delta r_{i+1}} \right)}^{\text{from cell } \mathbf{I}+2\mathbf{e}_r} \underbrace{+\Delta r_i \Delta\theta \Delta z_k \left(\frac{2 r_{i+\frac{1}{2}} u_{r_{\mathbf{I}+\mathbf{e}_r}}}{\Delta r_i + \Delta r_{i+1}} - \frac{2 r_{i-\frac{1}{2}} u_{r_{\mathbf{I}-\mathbf{e}_r}}}{\Delta r_{i-1} + \Delta r_i} \right)}_{\text{from cell } \mathbf{I}} \Bigg], \tag{110}$$

which after simplification reduces to $-\Delta\theta \Delta z_k \left(r_{i+\frac{1}{2}} u_{r_{\mathbf{I}+\mathbf{e}_r}} - r_{i-\frac{1}{2}} u_{r_{\mathbf{I}-\mathbf{e}_r}} \right)$. In a similar fashion, collecting all angular contributions to $p_\mathbf{I}$ gives:

$$-\frac{\Delta r_i \Delta z_k}{2} \Bigg[\overbrace{-u_{\theta_{\mathbf{I}-\mathbf{e}_\theta}}}^{\text{from cell } \mathbf{I}-2\mathbf{e}_\theta} \underbrace{-u_{\theta_{\mathbf{I}-\mathbf{e}_\theta}} + u_{\theta_{\mathbf{I}+\mathbf{e}_\theta}}}_{\text{from cell } \mathbf{I}} \overbrace{+u_{\theta_{\mathbf{I}+\mathbf{e}_\theta}}}^{\text{from cell } \mathbf{I}+2\mathbf{e}_\theta} \Bigg], \tag{111}$$

which reduces to $-\Delta r_i \Delta z_k (u_{\theta_{\mathbf{I}+\mathbf{e}_\theta}} - u_{\theta_{\mathbf{I}-\mathbf{e}_\theta}})$. Finally, for the axial contributions, we get:

$$-\frac{r_i \Delta r_i \Delta\theta}{2} \Bigg[\overbrace{-\frac{2\Delta z_{k-1}}{\Delta z_{k-1} + \Delta z_k} u_{z_{\mathbf{I}-\mathbf{e}_z}}}^{\text{from cell } \mathbf{I}-2\mathbf{e}_z} \overbrace{-\frac{2\Delta z_k}{\Delta z_{k-1} + \Delta z_k} u_{z_{\mathbf{I}-\mathbf{e}_z}} + \frac{2\Delta z_k}{\Delta z_k + \Delta z_{k+1}} u_{z_{\mathbf{I}+\mathbf{e}_z}}}^{\text{from cell } \mathbf{I}} \overbrace{+\frac{2\Delta z_{k+1}}{\Delta z_k + \Delta z_{k+1}} u_{z_{\mathbf{I}+\mathbf{e}_z}}}^{\text{from cell } \mathbf{I}+2\mathbf{e}_z} \Bigg], \tag{112}$$

which reduces to $-r_i \Delta r_i \Delta\theta (u_{z_{\mathbf{I}+\mathbf{e}_z}} - u_{z_{\mathbf{I}-\mathbf{e}_z}})$. Comparing the coefficient for $p_\mathbf{I}$ from equation (108) and the cumulative coefficient from equations (110), (111) and (112) shows that after summation over the entire computational grid it holds that $(\mathbf{Du}, p)_{HC} = -(\mathbf{u}, \overline{\mathbf{G}}p)_{\mathcal{HS}}$. □

Proposition. *For any $\boldsymbol{\omega} \in \mathcal{HL}$ and $\mathbf{u} \in \mathcal{HS}$ on an infinite domain, it holds that* $(\mathbf{C}\boldsymbol{\omega}, \mathbf{u})_{\mathcal{HS}} = (\boldsymbol{\omega}, \overline{\mathbf{C}}\mathbf{u})_{\mathcal{HL}}$.

Proof. Let $\boldsymbol{\omega} = (\eta, \omega, \zeta) \in \mathcal{HL}$ and $\mathbf{u} = (u_r, u_\theta, u_z) \in \mathcal{HS}$. We collect the components of $\boldsymbol{\omega}$ in both inner products. For $\eta_{\mathbf{I}+\mathbf{e}_\theta+\mathbf{e}_z}$, there are contributions from cells $\mathbf{I}$, $\mathbf{I}+2\mathbf{e}_\theta$, $\mathbf{I}+2\mathbf{e}_z$ and $\mathbf{I}+2\mathbf{e}_\theta+2\mathbf{e}_z$. The sum of the contributions to the term $\eta_{\mathbf{I}+\mathbf{e}_\theta+\mathbf{e}_z}$ from the inner product $(\mathbf{C}\boldsymbol{\omega}, \mathbf{u})_{\mathcal{HS}}$ is:

$$\frac{r_i \Delta r_i \Delta\theta \Delta z_k}{2}\left[\overbrace{\frac{u_{\theta_{\mathbf{I}+\mathbf{e}_\theta}}}{\Delta z_k} - \frac{u_{z_{\mathbf{I}+\mathbf{e}_z}}}{r_i\Delta\theta}}^{\text{from cell } \mathbf{I}} + \overbrace{\frac{u_{\theta_{\mathbf{I}+\mathbf{e}_\theta}}}{\Delta z_k} + \frac{u_{z_{\mathbf{I}+2\mathbf{e}_\theta+\mathbf{e}_z}}}{r_i\Delta\theta}}^{\text{from cell } \mathbf{I}+2\mathbf{e}_\theta}\right]$$

$$+\frac{r_i \Delta r_i \Delta\theta \Delta z_{k+1}}{2}\left[\underbrace{-\frac{u_{\theta_{\mathbf{I}+\mathbf{e}_\theta+2\mathbf{e}_z}}}{\Delta z_{k+1}} - \frac{u_{z_{\mathbf{I}+\mathbf{e}_z}}}{r_i\Delta\theta}}_{\text{from cell } \mathbf{I}+2\mathbf{e}_z} \underbrace{-\frac{u_{\theta_{\mathbf{I}+\mathbf{e}_\theta+2\mathbf{e}_z}}}{\Delta z_{k+1}} + \frac{u_{z_{\mathbf{I}+2\mathbf{e}_\theta+\mathbf{e}_z}}}{r_i\Delta\theta}}_{\text{from cell } \mathbf{I}+2\mathbf{e}_\theta+2\mathbf{e}_z}\right], \tag{113}$$

which reduces to

$$r_i \Delta r_i \Delta\theta \frac{\Delta z_k + \Delta z_{k+1}}{2}\left(\frac{u_{z_{\mathbf{I}+2\mathbf{e}_\theta+ez}} - u_{z_{\mathbf{I}+ez}}}{r_i\Delta\theta} - \frac{2(u_{\theta_{\mathbf{I}+\mathbf{e}_\theta+2\mathbf{e}_z}} - u_{\theta_{\mathbf{I}+\mathbf{e}_\theta}})}{\Delta z_k + \Delta z_{k+1}}\right). \tag{114}$$

The contributions from the inner product $(\boldsymbol{\omega}, \bar{\mathbf{C}}\mathbf{u})_{\mathcal{HL}}$ consist of:

$$\left[2\cdot\overbrace{\frac{r_i \Delta r_i \Delta\theta \Delta z_k}{2}}^{\text{from cells } \mathbf{I},\ \mathbf{I}+2\,\mathbf{e}_\theta} + 2\cdot\overbrace{\frac{r_i \Delta r_i \Delta\theta \Delta z_{k+1}}{2}}^{\text{from cells } \mathbf{I}+2\mathbf{e}_z, \mathbf{I}+2\mathbf{e}_\theta+2\mathbf{e}_z}\right]\frac{(\bar{\mathbf{C}}\mathbf{u})_{r_{\mathbf{I}+\mathbf{e}_\theta+\mathbf{e}_z}}}{2} = r_i \Delta r_i \Delta\theta \frac{\Delta z_k + \Delta z_{k+1}}{2}(\bar{\mathbf{C}}\mathbf{u})_{r_{\mathbf{I}+\mathbf{e}_\theta+\mathbf{e}_z}}, \tag{115}$$

which after substitution of equation (44) becomes exactly equation (114). Hence, for an arbitrary $\eta_{\mathbf{I}+\mathbf{e}_\theta+\mathbf{e}_z}$, both inner products yield the same contributions. Then we collect all contributions to $\omega_{\mathbf{I}+\mathbf{e}_r+\mathbf{e}_z}$. These come from cells $\mathbf{I}$, $\mathbf{I}+2\mathbf{e}_r$, $\mathbf{I}+2\mathbf{e}_z$ and $\mathbf{I}+2\mathbf{e}_r+2\mathbf{e}_z$. From the inner product $(\mathbf{C}\boldsymbol{\omega}, \mathbf{u})_{\mathcal{HS}}$, we get:

$$\frac{r_{i+\frac{1}{2}}\Delta\theta}{2}\left[\overbrace{-\Delta r_i u_{r_{\mathbf{I}+\mathbf{e}_r}} + \Delta z_k u_{z_{\mathbf{I}+\mathbf{e}_z}}}^{\text{from cell } \mathbf{I}} \overbrace{-\Delta r_{i+1} u_{r_{\mathbf{I}+\mathbf{e}_r}} - \Delta z_k u_{z_{\mathbf{I}+2\mathbf{e}_r+\mathbf{e}_z}}}^{\text{from cell } \mathbf{I}+2\mathbf{e}_r}\right. \tag{116}$$

$$\left. + \underbrace{\Delta r_i u_{r_{\mathbf{I}+\mathbf{e}_r+2\,\mathbf{e}_z}} + \Delta z_{k+1} u_{z_{\mathbf{I}+\mathbf{e}_z}}}_{\text{from cell } \mathbf{I}+2\mathbf{e}_z} + \underbrace{\Delta r_{i+1} u_{r_{\mathbf{I}+\mathbf{e}_r+2\mathbf{e}_z}} - \Delta z_{k+1} u_{z_{\mathbf{I}+2\mathbf{e}_r+\mathbf{e}_z}}}_{\text{from cell } \mathbf{I}+2\mathbf{e}_r+2\mathbf{e}_z}\right],$$

which reduces to:

$$r_{i+\frac{1}{2}}\frac{\Delta r_i + \Delta r_{i+1}}{2}\Delta\theta\frac{\Delta z_k + \Delta z_{k+1}}{2}\left(\frac{2(u_{r_{\mathbf{I}+\mathbf{e}_r+2\mathbf{e}_z}} - u_{r_{\mathbf{I}+\mathbf{e}_r}})}{\Delta z_k + \Delta z_{k+1}} - \frac{2\left(u_{z_{\mathbf{I}+2\mathbf{e}_r+\mathbf{e}_z}} - u_{z_{\mathbf{I}+\mathbf{e}_z}}\right)}{\Delta r_i + \Delta r_{i+1}}\right). \tag{117}$$

From the inner product $(\boldsymbol{\omega}, \bar{\mathbf{C}}\mathbf{u})_{\mathcal{HL}}$, we collect:

$$\left[\overbrace{\frac{r_{i+\frac{1}{2}}\Delta r_i \Delta\theta \Delta z_k}{4}}^{\text{from cell } \mathbf{I}} + \overbrace{\frac{r_{i+\frac{1}{2}}\Delta r_i \Delta\theta \Delta z_{k+1}}{4}}^{\text{from cell } \mathbf{I}+2\mathbf{e}_z} + \overbrace{\frac{r_{i+\frac{1}{2}}\Delta r_{i+1} \Delta\theta \Delta z_k}{4}}^{\text{from cell } \mathbf{I}+2\mathbf{e}_r} + \overbrace{\frac{r_{i+\frac{1}{2}}\Delta r_{i+1} \Delta\theta \Delta z_{k+1}}{4}}^{\text{from cell } \mathbf{I}+2\mathbf{e}_r+2\,\mathbf{e}_z}\right](\bar{\mathbf{C}}\mathbf{u})_{\theta_{\mathbf{I}+\mathbf{e}_r+\mathbf{e}_z}} \tag{118}$$

$$= r_{i+\frac{1}{2}}\frac{\Delta r_i + \Delta r_{i+1}}{2}\Delta\theta\frac{\Delta z_k + \Delta z_{k+1}}{2}(\bar{\mathbf{C}}\mathbf{u})_{\theta_{\mathbf{I}+\mathbf{e}_r+\mathbf{e}_z}}. \tag{119}$$

After substitution of $(\bar{\mathbf{C}}\mathbf{u})_{\theta_{\mathbf{I}+\mathbf{e}_r+\mathbf{e}_z}}$ from equation (46), we get exactly the result of equation (117). Finally, collecting all contributions to $\zeta_{\mathbf{I}+\mathbf{e}_r+\mathbf{e}_\theta}$ from cells $\mathbf{I}$, $\mathbf{I}+2\mathbf{e}_r$, $\mathbf{I}+2\mathbf{e}_\theta$ and $\mathbf{I}+2\mathbf{e}_r+2\mathbf{e}_\theta$, we get from the inner product $(\mathbf{C}\boldsymbol{\omega}, \mathbf{u})_{\mathcal{HS}}$:

$$\frac{\Delta z_k}{2}\left[\overbrace{\Delta r_i u_{r_{\mathbf{I}+\mathbf{e}_r}} - r_i\Delta\theta u_{\theta_{\mathbf{I}+\mathbf{e}_\theta}}}^{\text{from cell } \mathbf{I}} + \overbrace{\Delta r_{i+1} u_{r_{\mathbf{I}+\mathbf{e}_r}} + r_{i+1}\Delta\theta u_{\theta_{\mathbf{I}+2\mathbf{e}_r+\mathbf{e}_\theta}}}^{\text{from cell } \mathbf{I}+2\mathbf{e}_r}\right. \tag{120}$$

$$\left. \underbrace{-\Delta r_i u_{r_{\mathbf{I}+\mathbf{e}_r+2\,\mathbf{e}_\theta}} - r_i\Delta\theta u_{\theta_{\mathbf{I}+\mathbf{e}_\theta}}}_{\text{from cell } \mathbf{I}+2\,\mathbf{e}_\theta} \underbrace{-\Delta r_{i+1} u_{r_{\mathbf{I}+\mathbf{e}_\theta+2\mathbf{e}_\theta}} + r_{i+1}\Delta\theta u_{\theta_{\mathbf{I}+2\mathbf{e}_r+\mathbf{e}_\theta}}}_{\text{from cell } \mathbf{I}+2\mathbf{e}_r+2\mathbf{e}_\theta}\right],$$

which reduces to

$$\frac{\Delta r_i + \Delta r_{i+1}}{2}\Delta\theta\Delta z_k\left(\frac{2\left(r_{i+1}u_{\theta_{\mathbf{I}+2\mathbf{e}_r+\mathbf{e}_\theta}} - r_i u_{\theta_{\mathbf{I}+\mathbf{e}_\theta}}\right)}{\Delta r_i + \Delta r_{i+1}} - \frac{u_{r_{\mathbf{I}+\mathbf{e}_r+2\mathbf{e}_\theta}} - u_{r_{\mathbf{I}+\mathbf{e}_r}}}{\Delta\theta}\right). \tag{121}$$

From the inner product $(\boldsymbol{\omega}, \overline{\mathbf{C}}\mathbf{u})_{\mathcal{HL}}$, we collect:

$$\left[\overbrace{\frac{r_i + r_{i+1}}{2} \frac{\Delta r_i \Delta\theta \Delta z_k}{2}}^{\text{from cells } \mathbf{I} \text{ and } \mathbf{I}+2\mathbf{e}_\theta} + \overbrace{\frac{r_i + r_{i+1}}{2} \frac{\Delta r_{i+1} \Delta\theta \Delta z_k}{2}}^{\text{from cells } \mathbf{I}+2\mathbf{e}_r \text{ and } \mathbf{I}+2\mathbf{e}_r+2\mathbf{e}_\theta} \right] (\overline{\mathbf{C}}\mathbf{u})_{z_{\mathbf{I}+\mathbf{e}_r+\mathbf{e}_\theta}} = \frac{r_i + r_{i+1}}{2} \frac{\Delta r_i + \Delta r_{i+1}}{2} \Delta\theta \Delta z_k (\overline{\mathbf{C}}\mathbf{u})_{z_{\mathbf{I}+\mathbf{e}_r+\mathbf{e}_\theta}}. \quad (122)$$

After substitution of equation (48), the resulting expression is exactly equation (121). For the specific case of $\widetilde{\zeta}_{k_0}$, the inner product $(\mathbf{C}\boldsymbol{\omega}, \mathbf{u})_{\mathcal{HS}}$ get contributions from all cells around the axis:

$$\frac{r_1 \Delta r_i \Delta\theta \Delta z_{k_0}}{2} \sum_{\mathbf{I}, i=1, k=k_0} \frac{u_{\theta_{\mathbf{I}+\mathbf{e}_\theta}} + u_{\theta_{\mathbf{I}-\mathbf{e}_\theta}}}{\Delta r_i} = r_1 \Delta\theta \Delta z_{k_0} \sum_{\mathbf{I}, i=1, k=k_0} u_{\theta_{\mathbf{I}+\mathbf{e}_\theta}}, \quad (123)$$

while the inner product $(\boldsymbol{\omega}, \overline{\mathbf{C}}\mathbf{u})_{\mathcal{HL}}$ yields:

$$N_\theta \frac{r_1 \Delta r_1 \Delta\theta \Delta z_{k_0}}{4} (\overline{\mathbf{C}}\mathbf{u})_{z_{0,k_0}}, \quad (124)$$

and after substitution of equation (49), this gives:

$$N_\theta \frac{r_1 \Delta r_1 \Delta\theta \Delta z_{k_0}}{4} \frac{4}{\Delta r_1 N_\theta} \sum_{\mathbf{I}, i=1, k=k_0} u_{\theta_{\mathbf{I}+\mathbf{e}_\theta}} = r_1 \Delta\theta \Delta z_{k_0} \sum_{\mathbf{I}, i=1, k=k_0} u_{\theta_{\mathbf{I}+\mathbf{e}_\theta}}, \quad (125)$$

which is precisely equation (123). □

References

[1] A. Abba, L. Bonaventura, A mimetic finite difference discretization for the incompressible Navier–Stokes equations, Int. J. Numer. Methods Fluids 56 (8) (2008) 1101–1106.
[2] E. Barbosa, O. Daube, A finite difference method for 3D incompressible flows in cylindrical coordinates, Comput. Fluids 34 (8) (2005) 950–971.
[3] O. Desjardins, G. Blanquart, G. Balarac, H. Pitsch, High order conservative finite difference scheme for variable density low Mach number turbulent flows, J. Comput. Phys. 227 (15) (2008) 7125–7159.
[4] J.G.M. Eggels, Direct and large eddy simulation of turbulent flow in a cylindrical pipe geometry, PhD thesis, Delft University of Technology, 1994.
[5] K. Fukagata, N. Kasagi, Highly energy-conservative finite difference method for the cylindrical coordinate system, J. Comput. Phys. 181 (2) (2002) 478–498.
[6] M.D. Griffin, E. Jones, J.D. Anderson, A computational fluid dynamic technique valid at the centerline for non-axisymmetric problems in cylindrical coordinates, J. Comput. Phys. 30 (3) (1979) 352–360.
[7] F.H. Harlow, J.E. Welch, Numerical calculation of time-dependent viscous incompressible flow of fluid with free surface, Phys. Fluids 8 (12) (1965) 2182.
[8] J.M. Hyman, M. Shashkov, Adjoint operators for the natural discretizations of the divergence, gradient and curl on logically rectangular grids, Appl. Numer. Math. 25 (4) (1997) 413–442.
[9] J.M. Hyman, M. Shashkov, Natural discretizations for the divergence, gradient, and curl on logically rectangular grids, Comput. Math. Appl. 33 (4) (1997) 81–104.
[10] K. Lipnikov, G. Manzini, M. Shashkov, Mimetic finite difference method, J. Comput. Phys. 257 (2014) 1163–1227.
[11] Y. Morinishi, T.S. Lund, O.V. Vasilyev, P. Moin, Fully conservative higher order finite difference schemes for incompressible flow, J. Comput. Phys. 143 (1) (1998) 90–124.
[12] Y. Morinishi, O.V. Vasilyev, T. Ogi, Fully conservative finite difference scheme in cylindrical coordinates for incompressible flow simulations, J. Comput. Phys. 197 (2) (2004) 686–710.
[13] K. Salari, P. Knupp, Code verification by the method of manufactured solutions, Technical report, Sandia National Labs, Albuquerque, NM (US), Livermore, CA (US), 2000.
[14] M. Shashkov, Conservative Finite-Difference Schemes on General Grids, 1995.
[15] R.W.C.P. Verstappen, A.E.P. Veldman, Symmetry-preserving discretization of turbulent flow, J. Comput. Phys. 187 (1) (2003) 343–368.
[16] R. Verzicco, P. Orlandi, A finite-difference scheme for three-dimensional incompressible flows in cylindrical coordinates, J. Comput. Phys. 123 (2) (1996) 402–414.
[17] M. Vinokur, Conservation equations of gasdynamics in curvilinear coordinate systems, J. Comput. Phys. 14 (2) (1974) 105–125.